TECHNICAL MEMORANDUM

X-645

SUBSONIC AERODYNAMIC CHARACTERISTICS OF PYRAMIDAL RE-ENTRY SHAPES INCORPORATING VARIABLE GEOMETRY

By Fred A. Demele and Jack J. Brownson

Ames Research Center
Moffett Field, Calif.

NATIONAL AERONAUTICS AND SPACE ADMINISTRATION
WASHINGTON
January 1962

1U

NATIONAL AERONAUTICS AND SPACE ADMINISTRATION

TECHNICAL MEMORANDUM X-645

SUBSONIC AERODYNAMIC CHARACTERISTICS OF PYRAMIDAL RE-ENTRY SHAPES INCORPORATING VARIABLE GEOMETRY*

By Fred A. Demele and Jack J. Brownson

SUMMARY

An investigation has been made to determine the aerodynamic characteristics of two blunt-nosed pyramidal re-entry shapes with square and rectangular cross sections, respectively, and large deflectable surfaces. The four sides of each body were hinged at approximately half the body length so that the rear surfaces were in the nature of four large flaps which permit lift and drag modulation in all stages of re-entry. At subsonic speeds, the upper and lower surfaces are deflected inward to reduce the base area, and hence the base drag, while the vertical surfaces serve as end plates which reduce the drag induced by lift. Upper surface elevons were provided for trimming the model with rectangular cross sections. The tests were conducted to maximum angles of attack of 25° and angles of sideslip of 19° over a range of Mach numbers from 0.20 to 0.90 at a Reynolds number of 3.3×10^{6} and at Reynolds numbers to 15×10^{6} at a Mach number of 0.20.

It was found that the square pyramidal model had linear lift and pitching-moment curves, but had very high drag. The drag could be reduced substantially by alining the movable vertical surfaces with the airstream, but at the expense of stability. The rectangular pyramidal model also had linear lift and pitching-moment curves. By proper positioning of the movable horizontal surfaces, longitudinal stability could be maintained throughout the subsonic speed range with the moment center located at 44 percent of the body length. The elevons were an effective means of providing trim change with only small reductions in lift-drag ratio. At low speeds and for a lift coefficient of 0.4, the trim lift-drag ratio was almost 4.5. A horizontal landing speed of 152 knots was calculated for a hypothetical re-entry vehicle based on the rectangular pyramidal model with a wing loading of 40 pounds per square foot. The model had static directional stability and positive effective dihedral throughout the Mach number range investigated.

*Title, Unclassified

INTRODUCTION

A vehicle entering the earth's atmosphere passes through several flight regimes, each imposing somewhat different design requirements which are difficult to reconcile efficiently in a vehicle of fixed geometry. By utilizing variable geometry, however, it appears possible to attain design compatibility more readily from the standpoints of aerodynamic heating and aerodynamics throughout the speed range. One shape of interest which incorporates variable geometry is a four-sided pyramid with blunt nose. The four sides of the body are hinged at about half the body length so that the rear surfaces are in the nature of large flaps. The shape in its basic form is thus compact and therefore easily adapted to a booster. With the variable-geometry features, it has the potential of good drag modulation at hypersonic speeds and appears suitable for conventional horizontal landing. Prior to and during the critical heating stage, variations in lift or drag would be effected by outward deflection of the surfaces as shown in the accompanying illustration. Analysis by Newtonian impact theory indicates that simultaneous outward deflection of all four flaps will increase the drag at hypersonic speeds as much as an order of magnitude, thus allowing deceleration to occur at high altitudes and thereby reducing the heating significantly (see, e.g., ref. 1). Subsequent to the critical heating stage, the top and bottom surfaces would be deflected differentially to provide control over lateral and longitudinal range. Prior to landing, the top and bottom surfaces would be deflected inward toward closure at the base with the vertical surfaces serving as end plates to minimize the drag. The lift-drag ratios associated with this type of arrangement were estimated to be sufficiently high to permit a conventional horizontal landing.

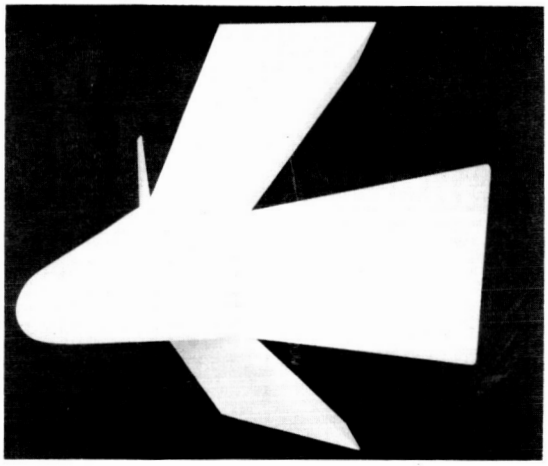

The investigation reported herein was undertaken to establish from aerodynamic considerations the feasibility of flight in the subsonic speed range, particularly in regard to horizontal landing capability. For this purpose, two pyramidal models were utilized. One model had square cross sections, the upper and lower surfaces being hinged at about half the body length to permit inward deflection of the rearward surfaces. The other model had a rectangular pyramidal shape to about half the body length with a constant span thereafter. The upper and lower surfaces were hinged at the line of surface discontinuity, again to permit inward deflection of the rearward surfaces. The tests were conducted in the Ames 12-Foot Pressure Wind Tunnel over a Mach number range from 0.20 to 0.90.

NOTATION

The data on the longitudinal characteristics are referred to the wind axes, and the data on the lateral-directional characteristics are referred to the body axes. The origin of the axes, or moment center, was located on the center line, 44 percent of the body length behind the nose.

a_n	normal acceleration, g
A	aspect ratio
b	span
C_D	drag coefficient, $\frac{\text{drag}}{qS}$
C_{D_o}	drag coefficient at zero lift
C_l	rolling-moment coefficient, $\frac{\text{rolling moment}}{qSb}$
C_L	lift coefficient, $\frac{\text{lift}}{qS}$
C_m	pitching-moment coefficient, $\frac{\text{pitching moment}}{qSl}$
C_n	yawing-moment coefficient, $\frac{\text{yawing moment}}{qSb}$
C_{p_b}	base pressure coefficient, $\frac{p_b - p}{q}$
C_Y	side-force coefficient, $\frac{\text{side force}}{qS}$
h	height of vertical surfaces at model base
l	model length
$\frac{L}{D}$	lift-drag ratio
M	free-stream Mach number
p	free-stream static pressure
p_b	base pressure
q	free-stream dynamic pressure
R	Reynolds number, based on model length

S	plan-form area
α	angle of attack, measured with respect to model center line
β	angle of sideslip
δ_e	elevon deflection angle (see fig. 3(b))
δ_L	lower surface deflection angle (see fig. 3)
δ_U	upper surface deflection angle (see fig. 3)
δ_V	vertical surface deflection angle (see fig. 3(a))

MODELS

Two models were tested in the investigation. One was a square pyramid with a blunt nose and a 20° apex angle (see figs. 1 and 3(a)). The upper and lower surfaces were hinged at about half the body length to permit varying degrees of closure at the base. Three sets of movable horizontal surfaces enabled the vertical surfaces behind the hinge line to be positioned at 10°, 5°, and 0° relative to the body center line. The other model differed in that it had rectangular cross sections and was pyramidal to approximately half the body length with a constant span thereafter (see figs. 2 and 3(b)). The upper and lower surfaces were hinged at the line of surface discontinuity to permit varying degrees of closure at the base. Elevons, or split flaps, having an area of 7 percent of the plan-form area, were utilized for trimming the model.

The models, which were supported by a 2.5-inch-diameter sting, enclosed a six-component strain-gage balance which was used to measure the forces and moments. A cylindrical fairing was used on the square pyramidal model to enclose the sting within the movable horizontal surfaces whenever the degree of base closure was less than the diameter of the sting (see fig. 1). This type fairing was also employed on the rectangular pyramidal model for conditions wherein the Reynolds number was varied and the flaps were differentially deflected; however, the preponderance of measurements for this model were made with the flaps cut out for sting clearance (see fig. 2(b)). Base pressures were measured with an orifice located adjacent to the sting and forward of the base of the sting fairing.

TESTS

The investigation was concerned primarily with the rectangular pyramidal shape. The tests were conducted with this model over a Mach number range of 0.20 to 0.90 at a Reynolds number (based on model length) of 3.3×10^6 and over a Reynolds number range of 3.3×10^6 to 15×10^6 at a Mach number of 0.20. Longitudinal characteristics were measured through an angle-of-attack range from -4° to $+25^\circ$, and lateral-directional characteristics were measured through an angle-of-sideslip range from -4° to $+19^\circ$ at angles of attack of 0°, 6°, and 12°. Results were obtained for several positions of the movable horizontal surfaces, ranging from fully open (base cross section rectangular) to fully closed at the base. Measurements were also made with elevons, or split flaps, attached to the upper surface. Tests of the square pyramidal model were conducted at a Mach number of 0.20 and a Reynolds number of 5×10^6 over an angle-of-attack range of -3° to $+25^\circ$. Results were obtained with the movable vertical surfaces at 0°, 5°, and 10° with respect to the plane of symmetry. Both models were tested in a clean condition, that is, without devices designed to fix the location of boundary-layer transition. The tests were conducted with the hinges and the intersection of the movable horizontal and vertical surfaces sealed.

CORRECTIONS TO DATA

The data have been corrected by the method of reference 2 for wind-tunnel-wall interference associated with lift on the model. The corrections which were added to the measured values are as follows:

$$\Delta\alpha = 0.2\ C_L$$

$$\Delta C_D = 0.003\ C_L^2$$

The effects of constriction due to the presence of the wind-tunnel walls were calculated by the method of reference 3. At a Mach number of 0.90, the correction amounted to an increase of about 1.5 percent in the measured value of Mach number and dynamic pressure.

No base-pressure corrections have been applied to the data; that is, the drag data have not been adjusted to correspond to a pressure at the base equal to free-stream static pressure.

RESULTS AND DISCUSSION

Square Pyramidal Model

The low-speed aerodynamic characteristics of the square pyramidal model are presented in figure 4 for the condition wherein the horizontal surfaces were closed at the base and the vertical surfaces were positioned at 10°, 5°, and 0° with respect to the body center line. It can be seen that the lift and pitching-moment curves were linear and that no sharp peak was evidenced in the lift-drag ratio curves. It is further evident that the aerodynamic characteristics were altered significantly by changes in the angle of the vertical surfaces. For example, decreasing the angle from 10° to 0° reduced the static longitudinal stability margin 10 percent of the body length and reduced the minimum drag 75 percent. Since the angle change was physically accomplished by decreasing the model span, which in turn resulted in a decreasing horizontal flap surface area, the reduction in stability can be related to the reduction in loading behind the hinge line. The large drag accompanying the model when the vertical surfaces are inclined to the airstream is quite likely a result of negative pressures in the region behind the hinge line acting on the inside of the vertical surfaces. Although the minimum drag decreased substantially with decreasing angle of the vertical surfaces, this decrease was not fully reflected in the lift-drag ratios. This is due primarily to increased induced drag associated with a reduction in aspect ratio. Thus, much higher values could be expected if the aspect ratio were not so low for the 0° position, for as shown in figure 5, while the induced drag was highest for the 0° position, it was only 50 percent of that calculated for an efficient lifting surface without end plates as indicated by the parameter $C_L^2/\pi A$. It is apparent that the end-plate effect of the vertical surfaces was significant in terms of increasing the effective aspect ratio.

On the basis of these data, it seemed quite clear that a pyramidal shape having vertical surfaces alined with the airstream and having an aspect ratio much larger than that of the square model with vertical surfaces positioned at 0° should have the necessary lift-drag characteristics required for conventional landing. These features were incorporated in the pyramidal shape having rectangular cross sections. The remaining discussion concerns the aerodynamic characteristics of this shape.

Rectangular Pyramidal Model

Low-speed longitudinal characteristics.- Longitudinal data at a Mach number of 0.2 are presented in figure 6 for upper and lower surface deflections of 25° (closure at the base) and Reynolds numbers from 3.3×10^6

to 15×10^6. The results indicate that increasing the Reynolds number resulted in slightly more linear lift and pitching-moment curves and in small increases in maximum lift-drag ratio. It is further evident that with the moment center located at 44 percent of the body length, the model exhibited a slight degree of static stability. Deflecting the horizontal surfaces outward from the 25° position, as shown in figures 7(a) and 7(b), resulted initially in a slight increase in stability followed by a decrease, such that with the surfaces at 0° the model was slightly unstable. In addition, both the lift-curve slope and lift-drag ratios decreased with decreasing surface angle. As shown in figure 7(c), it was possible to trim the model to lift coefficients of about 0.4 by differential deflection of the surfaces, with only small reductions in lift-drag ratio. With elevons, it was possible to trim the model to much higher lift coefficients than 0.4, again with only small reductions in lift-drag ratio (see fig. 8). At a lift coefficient of 0.4 the model had a trim lift-drag ratio of almost 4.5 with either of the two methods of trimming investigated.

The method of reference 4 was used to calculate a power-off landing approach for a hypothetical re-entry vehicle having the characteristics of the rectangular pyramidal model. The landing approach consisted of three phases: Phase I is a high-speed descent from altitude directed toward a ground reference point short of the runway; phase II is a constant g pull-out beginning at a specified speed and altitude and ending with the start of phase III, which is a shallow flight path along which the vehicle traverses to the touchdown point. The calculated landing approach is shown graphically in figure 9, which shows that for a wing loading of 40 pounds per square foot and a lift coefficient of 0.5 at touchdown, the velocity at touchdown was 152 knots. Thus, it appears that the performance of the assumed vehicle would be satisfactory for horizontal landing.

High subsonic speed longitudinal characteristics.- The longitudinal aerodynamic characteristics are presented in figure 10 for Mach numbers ranging from 0.60 to 0.90 and surface deflections ranging from 0° to 21°. At a Mach number of 0.60 (see fig. 10(a)) the effects of decreasing surface deflection were similar to those at low speeds; that is, the static stability, lift-curve slope, and lift-drag ratios generally decreased. At Mach numbers of 0.80 and above, these effects were evidenced generally between surface angles of 11° and 0°; however, at higher surface angles rather unexpected results were evidenced (see figs. 10(b), 10(c), and 10(d)). For a surface deflection of 21° (and, in fact, for 16° at a Mach number of 0.90) the lift was very small, or even negative up to angles of attack ranging from about 7° to 12°, above which the lift increased in the usual manner. In this low angle-of-attack region, the pitching moments were erratic and unstable. This phenomenon appears analagous to the results obtained at transonic speeds on a double-wedge airfoil (see ref. 5); that is, at Mach numbers near unity and at small positive angles of attack, the undersurface pressures behind the ridge

line were more negative than those on the upper surface. Thus, for the model described herein, the resultant negative lift on the region behind the hinge line would tend to negate the positive lift on the forebody, as well as to cause positive pitching moments.

Since, above Mach numbers of 0.60, a surface deflection of 11° appeared to be optimum from the standpoint of stability and lift-drag ratios, the elevons were investigated for this configuration. It may be seen in figure 11 that in the Mach number range from 0.60 to 0.90, an elevon deflection of 10° was effective in trimming the model to high lift coefficients.

Lateral-directional characteristics.- The low-speed lateral-directional characteristics are presented in figure 12 for the model with upper and lower surface deflections of 25°. The data show that the yawing-moment and side-force coefficients were little affected by angle of attack in the range from 0° to 12°, but that the rolling-moment coefficient increased nearly linearly with increasing angle of attack. It is apparent that the model had directional stability and positive effective dihedral at angles of attack greater than 0°. This favorable stability continued throughout the Mach number range as shown in figure 13, wherein data are presented for the model with upper and lower surface deflections of 11° at an angle of attack of 6°. It is noted that the coefficients generally increased smoothly with sideslip angle, the main exception being the rolling-moment coefficients, which decreased rather abruptly above a sideslip angle of 14° in the Mach number range from 0.80 to 0.90.

Base pressures.- The base pressure coefficients are presented in figure 14 as functions of angle of attack for various horizontal surface deflections. Characteristically, the base pressures become higher with increasing surface angle, that is, as the base area decreases. However, at high subsonic speeds a limiting surface angle exists for which the base pressures suddenly decrease at angles of attack less than about 12° (see fig. 14(b)). This phenomenon correlates with that noted previously concerning the lift and pitching-moment data.

CONCLUSIONS

The results of an investigation at Mach numbers from 0.20 to 0.90 of two pyramidal re-entry shapes with basically square and rectangular cross sections and with the horizontal surfaces hinged to permit varying degrees of closure at the base of the models can be summarized as follows:

1. The square pyramidal model had linear lift and pitching-moment curves, but had very high drag from the standpoint of conventional landing capability. Decreasing the angle between the movable vertical surfaces

[redacted]

and the model center line reduced the drag substantially, but resulted in reductions in longitudinal stability.

2. The rectangular pyramidal model, which had the vertical surfaces alined with the airstream and an increased aspect ratio, also had linear lift and pitching-moment curves. By proper positioning of the movable horizontal surfaces, longitudinal stability could be maintained throughout the subsonic speed range with the moment center located at 44 percent of the body length.

3. The rectangular pyramidal model could be trimmed throughout the Mach number range by the use of upper surface elevons, with only small reductions in lift-drag ratio. At low speeds and for a lift coefficient of 0.4, the model had a trim lift-drag ratio of almost 4.5.

4. A landing speed of 152 knots was calculated for a hypothetical re-entry vehicle based on the rectangular pyramidal model with a wing loading of 40 pounds per square foot.

5. The rectangular pyramidal model had directional stability and positive effective dihedral throughout the Mach number range investigated.

Ames Research Center
National Aeronautics and Space Administration
Moffett Field, Calif., Oct. 24, 1961

REFERENCES

1. Chapman, Dean R.: An Approximate Analytical Method for Studying Entry Into Planetary Atmospheres. NASA TR R-11, 1959. (Supersedes NACA TN 4276)

2. Glauert, Hermann: The Elements of Aerofoil and Airscrew Theory. Macmillan Company, N.Y., 1943, p. 191.

3. Herriot, John G.: Blockage Corrections for Three-Dimensional-Flow Closed Throat Wind Tunnels, With Consideration of the Effect of Compressibility. NACA Rep. 995, 1950. (Supersedes NACA RM A7B28, 1947)

4. Bray, Richard S., Drinkwater, Fred J., III, and White, Maurice D.: A Flight Study of a Power-Off Landing Technique Applicable to Re-entry Vehicles. NASA TN D-323, 1960.

5. Knechtel, Earl D.: Experimental Investigation at Transonic Speeds of Pressure Distributions Over Wedge and Circular-Arc Airfoil Sections and Evaluation of Perforated-Wall Interference. NASA TN D-15, 1959.

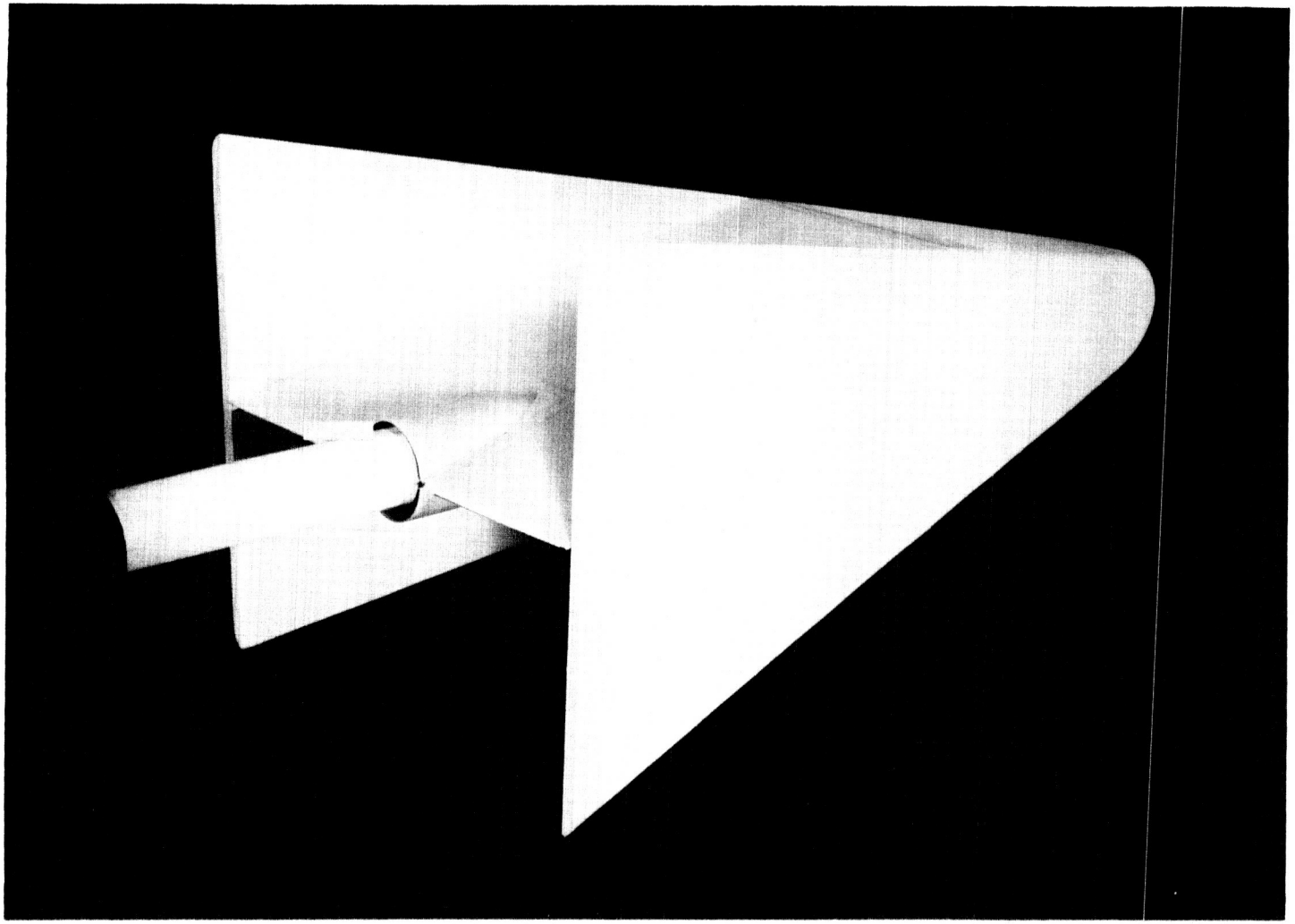

A-27992

(a) Rear view.

Figure 1.- Photographs of square pyramidal model.

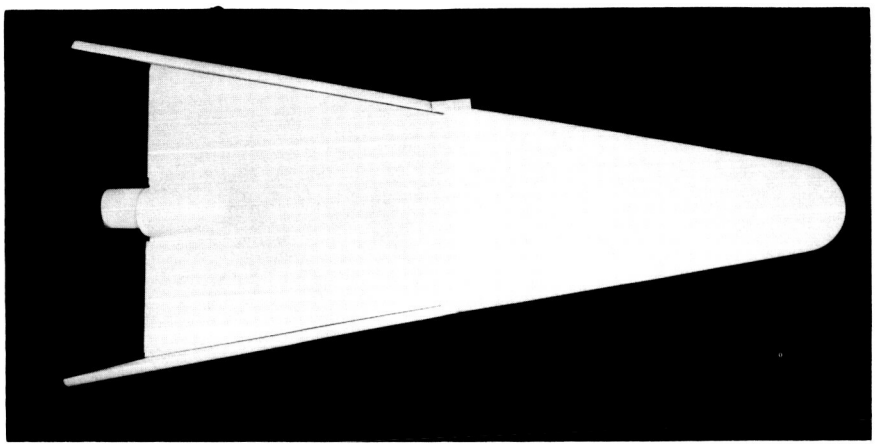

$\delta_V = 10^\circ$ A-27991

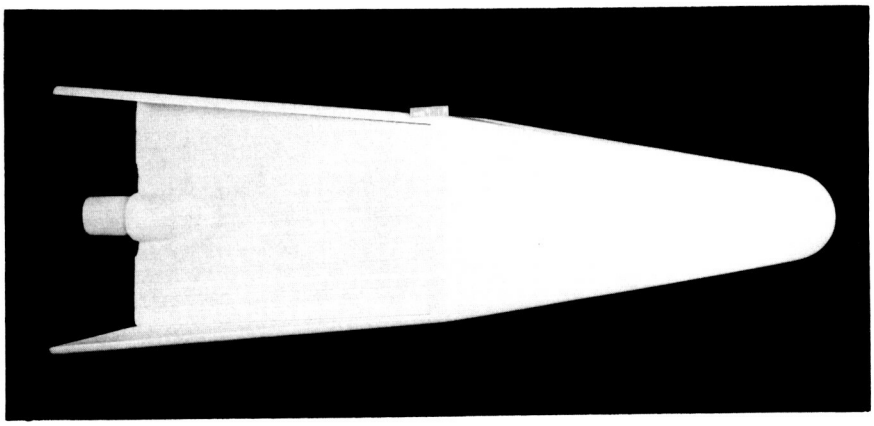

$\delta_V = 5^\circ$ A-27990

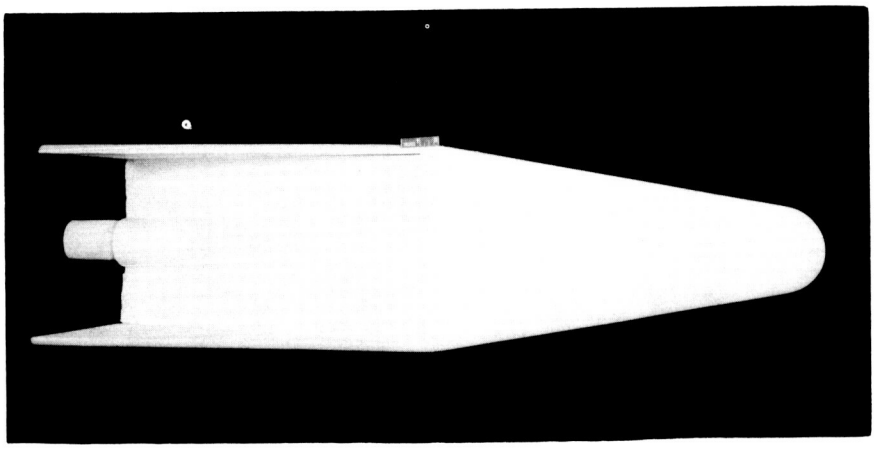

$\delta_V = 0^\circ$ A-27989

(b) Top views.

Figure 1.- Concluded.

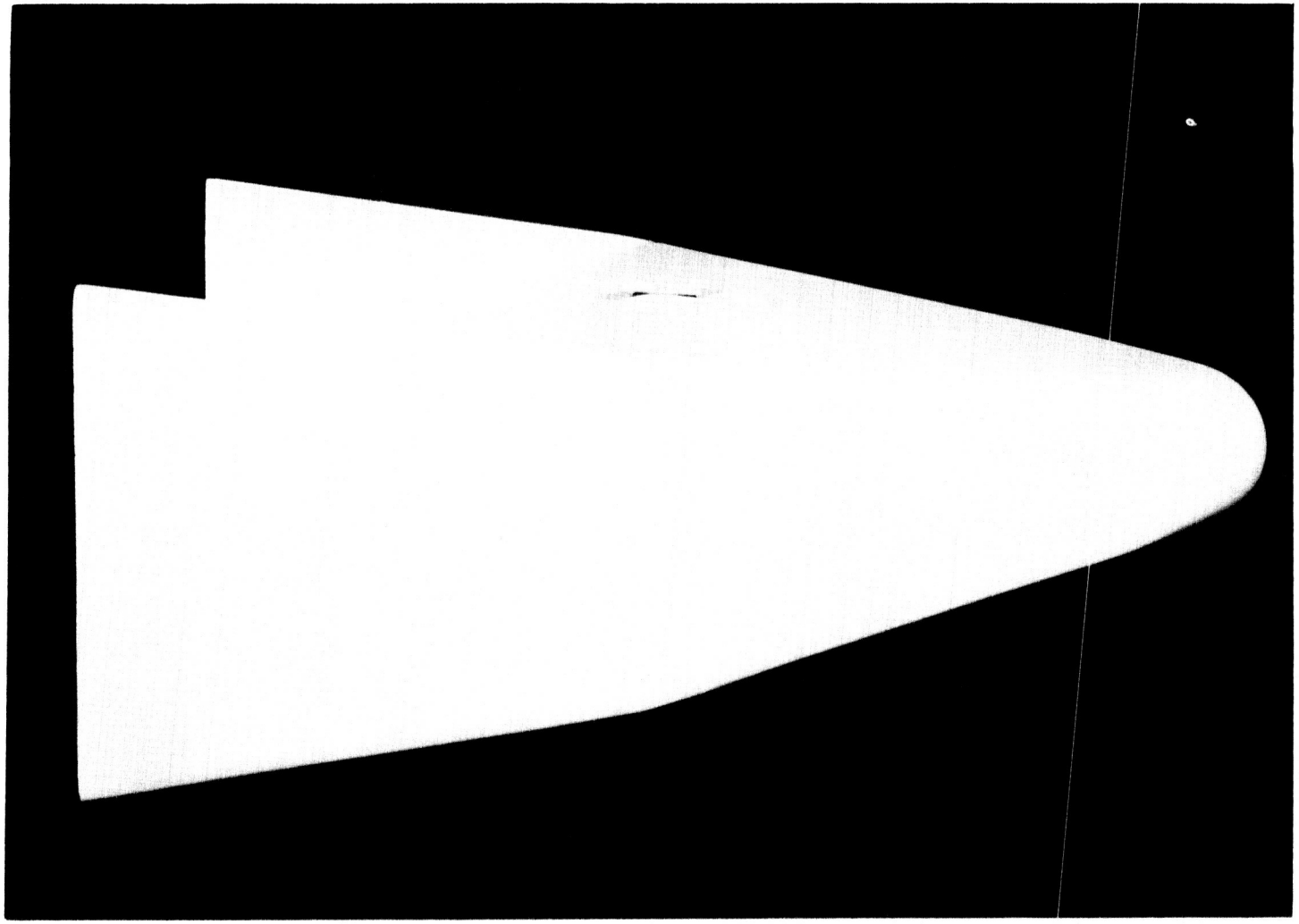

A-27984

(a) Side view.

Figure 2.- Photographs of rectangular pyramidal model.

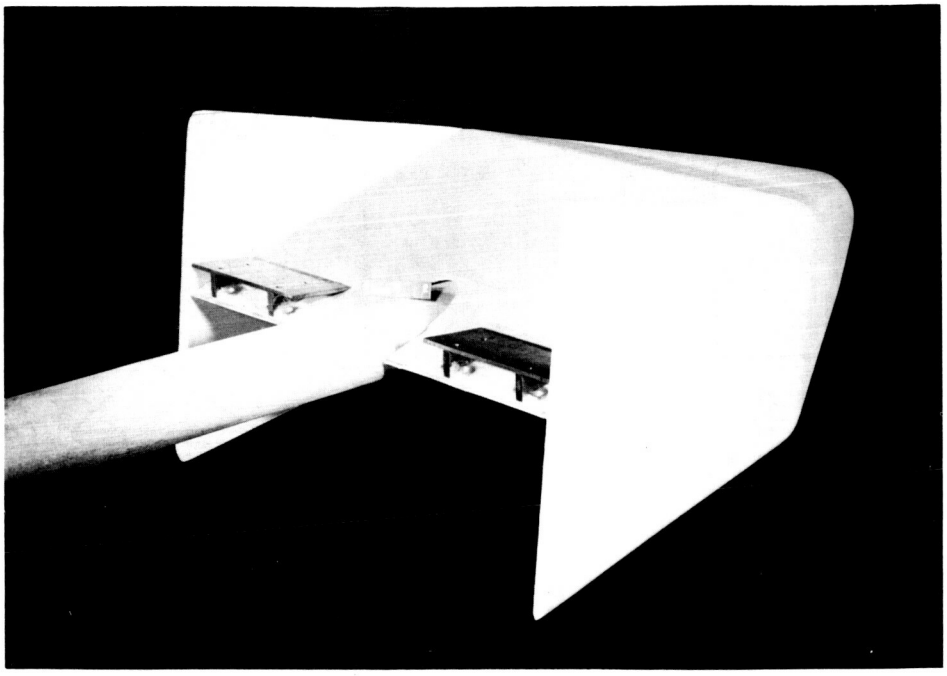

A-27986

With elevons

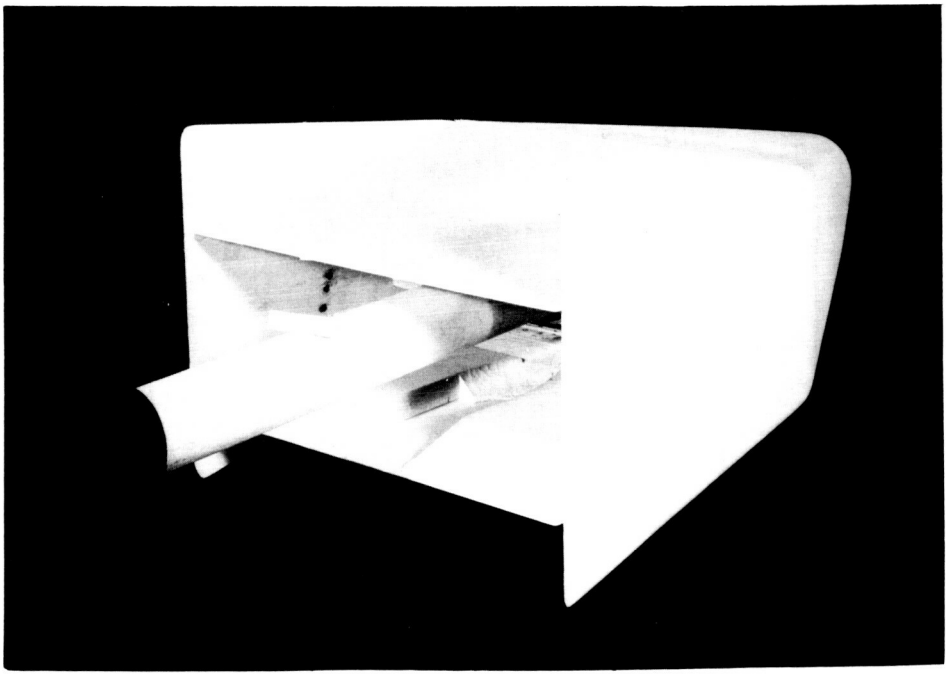

A-27987

Open base

(b) Rear views.

Figure 2.- Concluded.

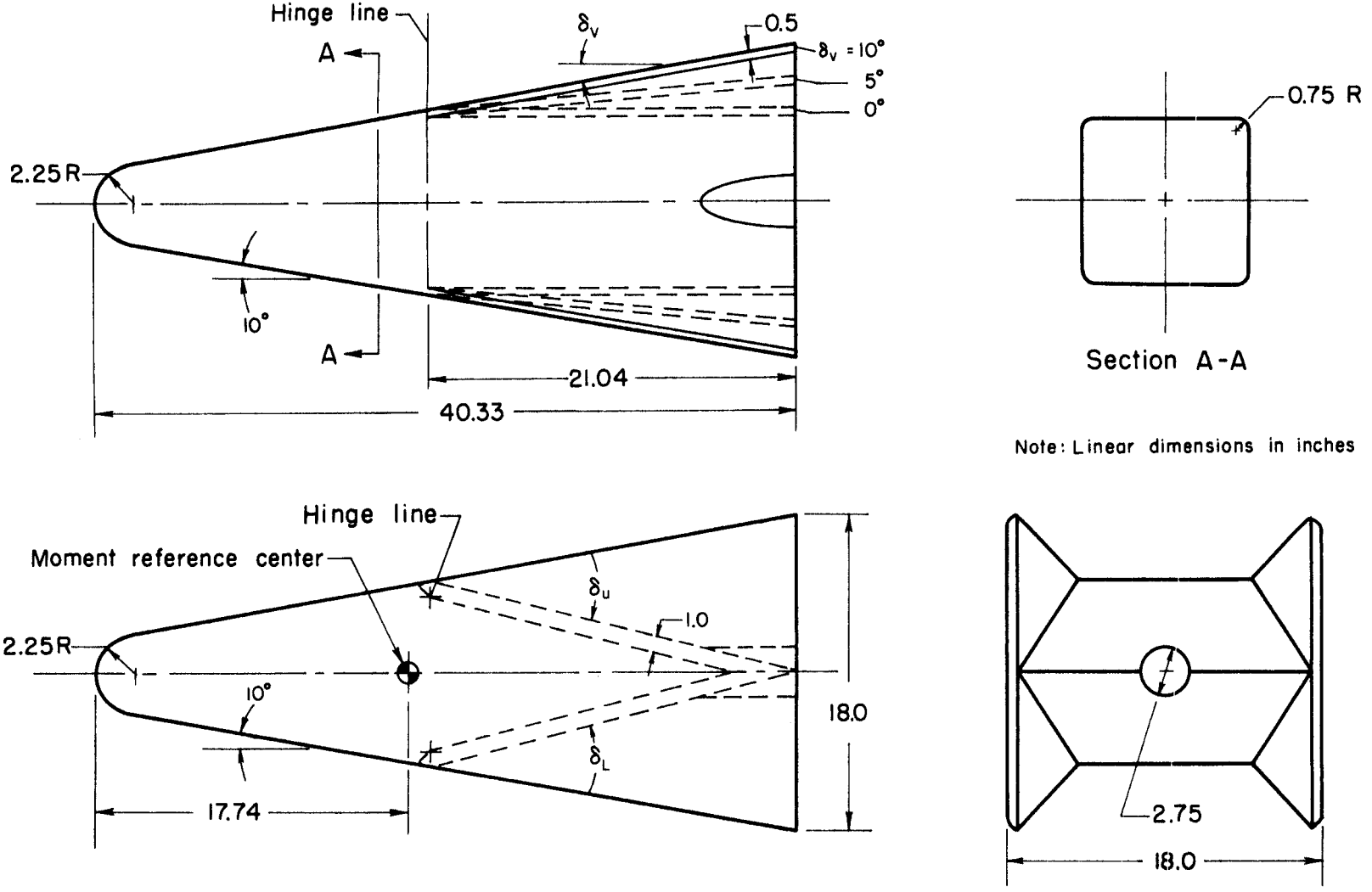

(a) Square pyramidal model.

Figure 3.- Geometric characteristics of the models.

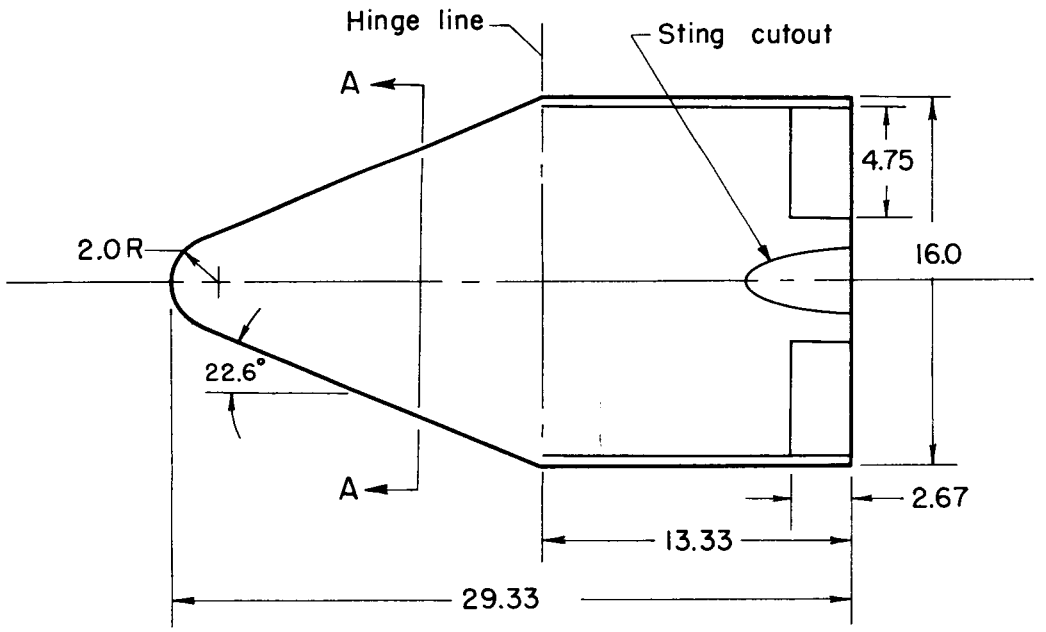

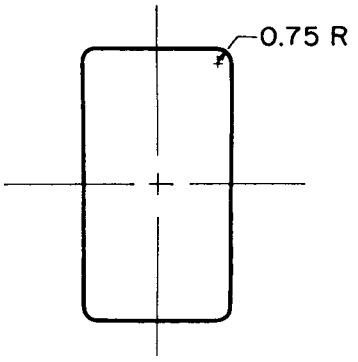

Section A-A

Note: Linear dimensions in inches

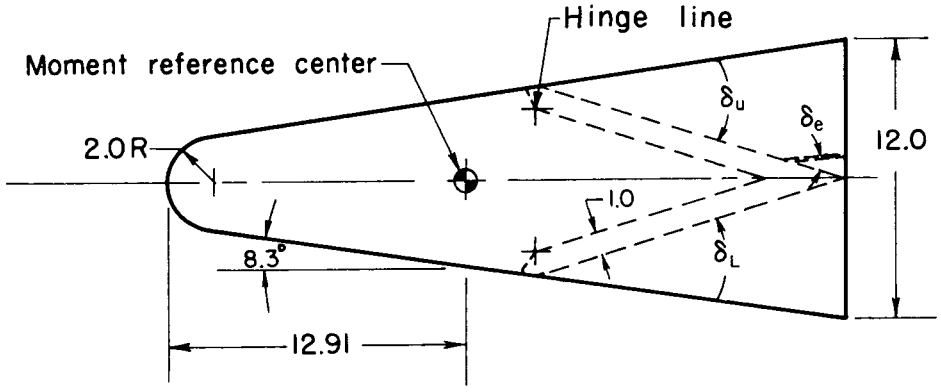

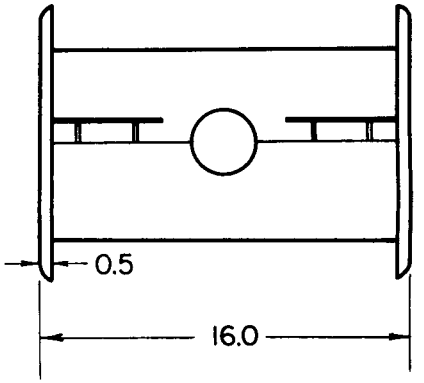

(b) Rectangular pyramidal model.

Figure 3.- Concluded.

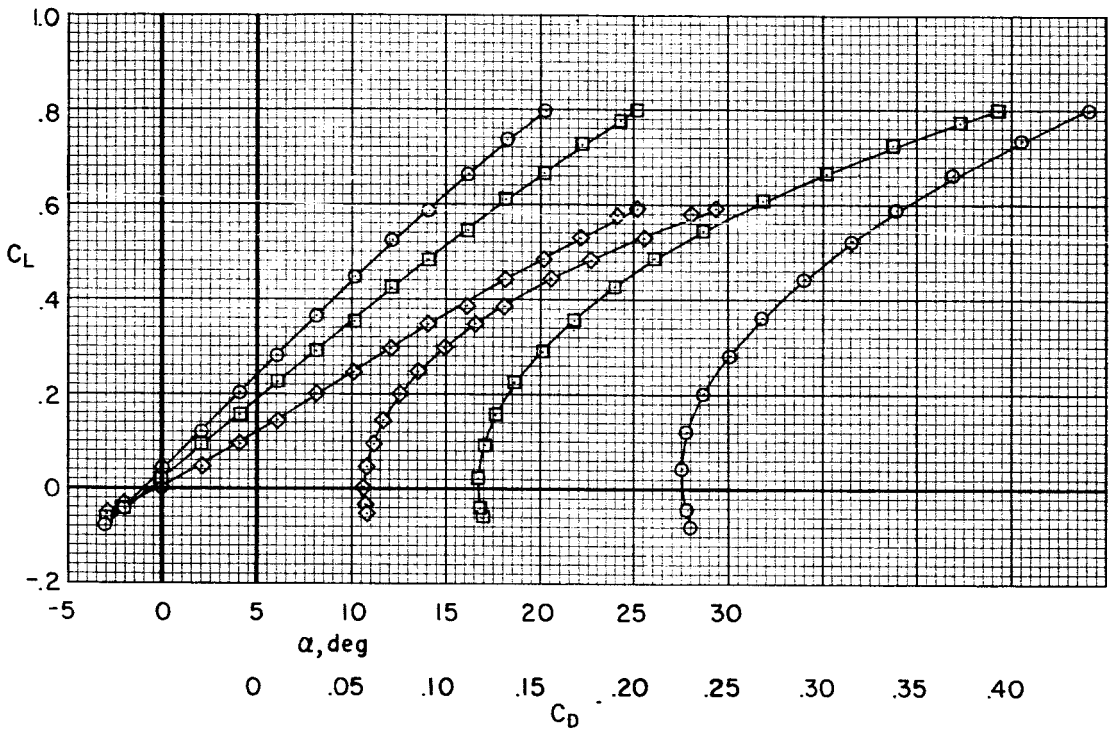

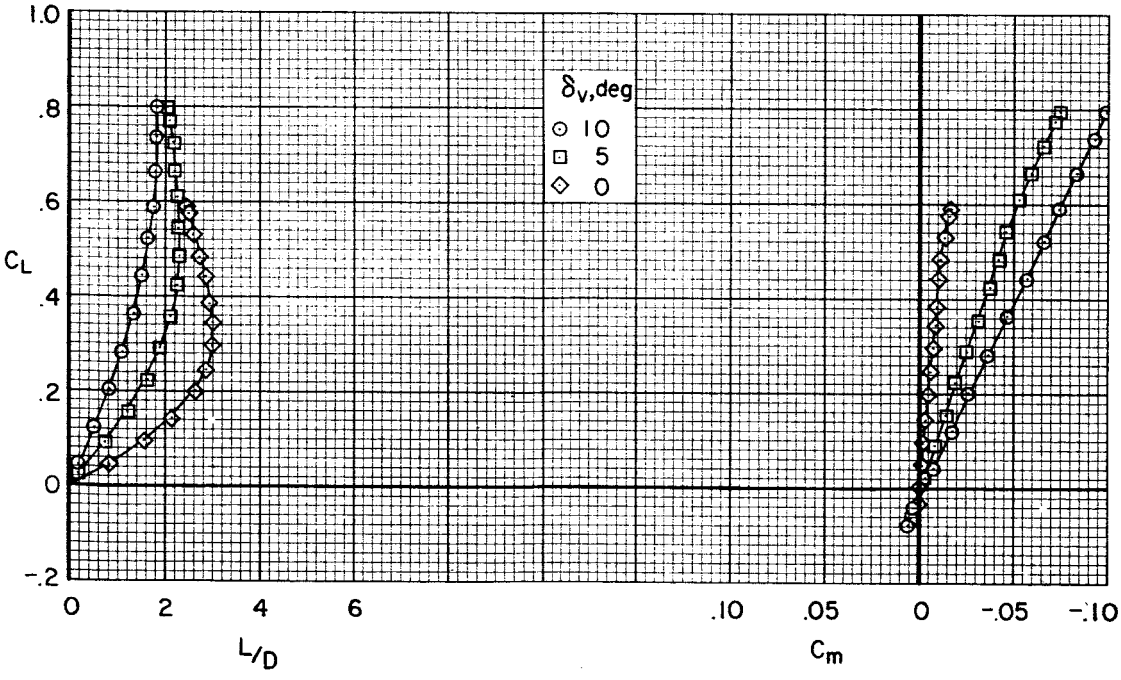

Figure 4.- Effect of angle of movable vertical surfaces on the low-speed aerodynamic characteristics of the square pyramidal model; δ_U, δ_L = 24°; M = 0.20; R = 5×10^6.

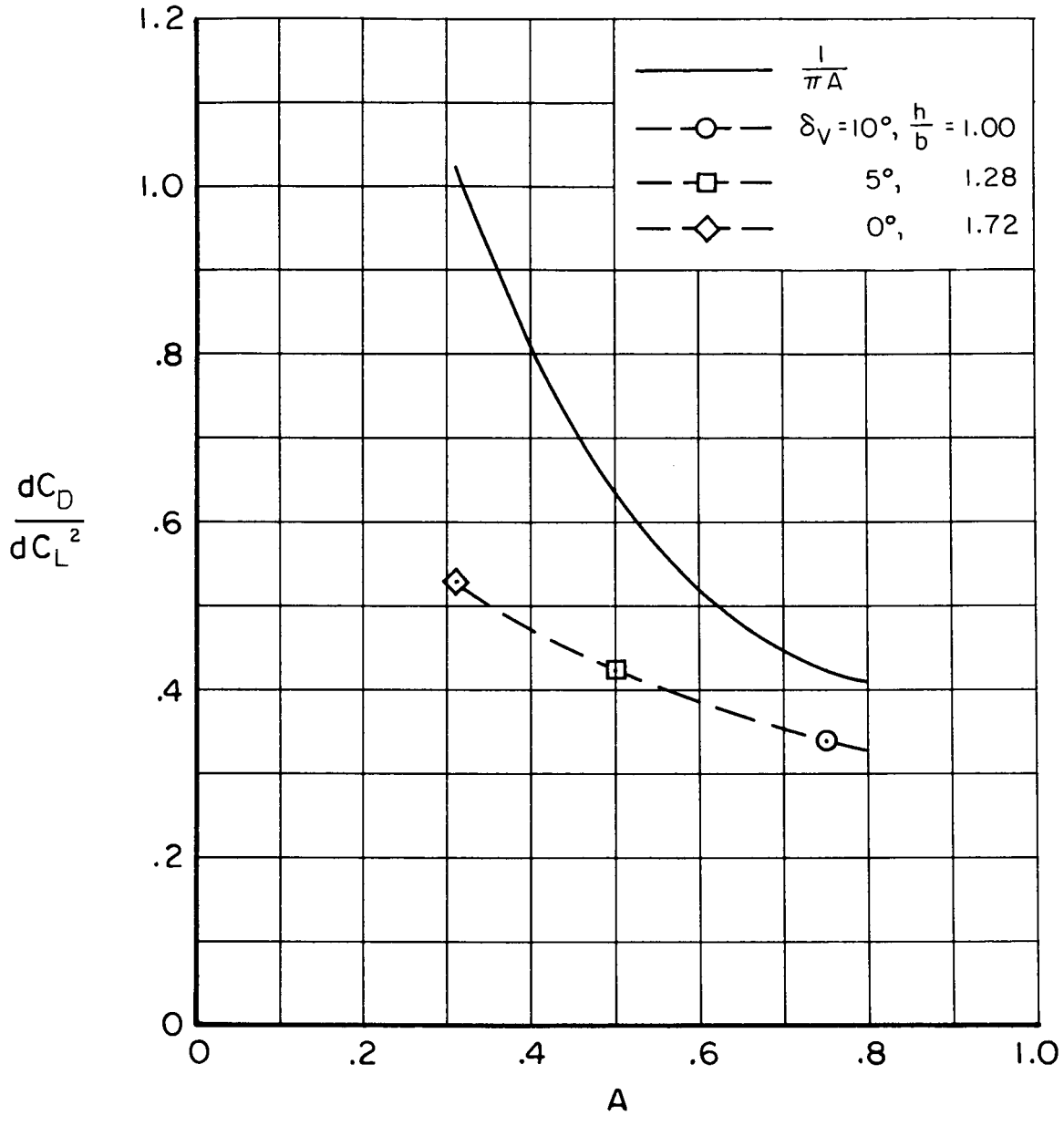

Figure 5.- Drag due to lift of the square pyramidal model; δ_U, $\delta_L = 24^\circ$; M = 0.20; R = 5×10^6.

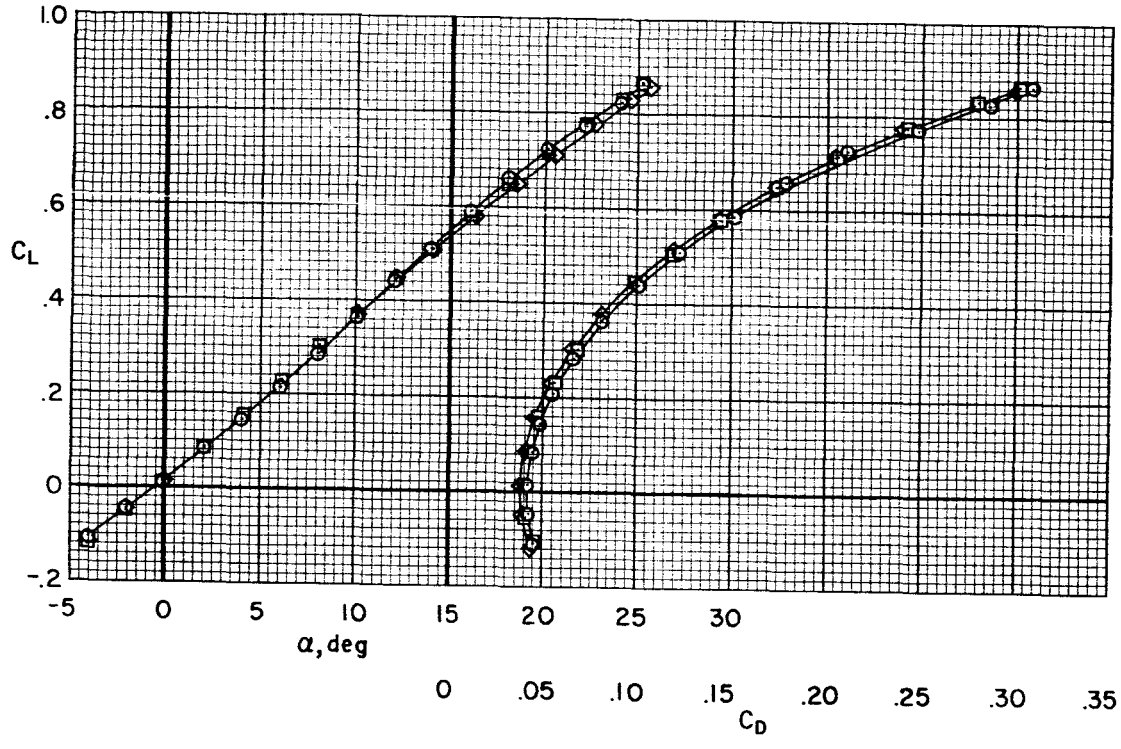

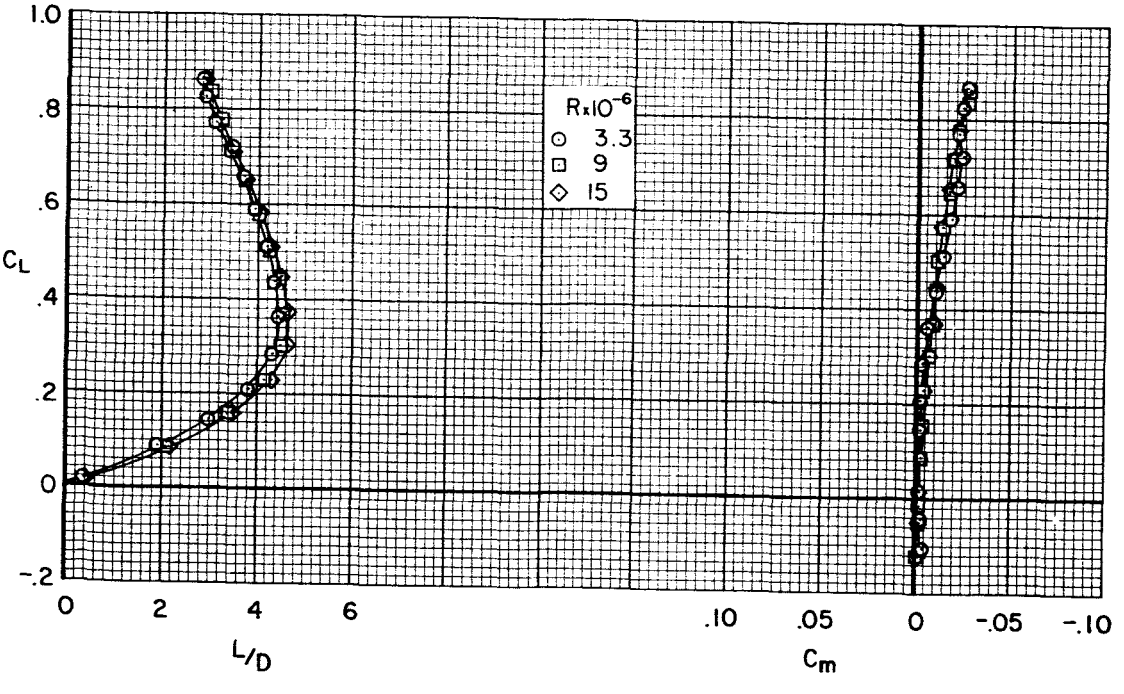

Figure 6.- The effects of Reynolds number on the low-speed aerodynamic characteristics of the rectangular pyramidal model; δ_U, $\delta_L = 25^\circ$; cylindrical sting fairing; M = 0.20.

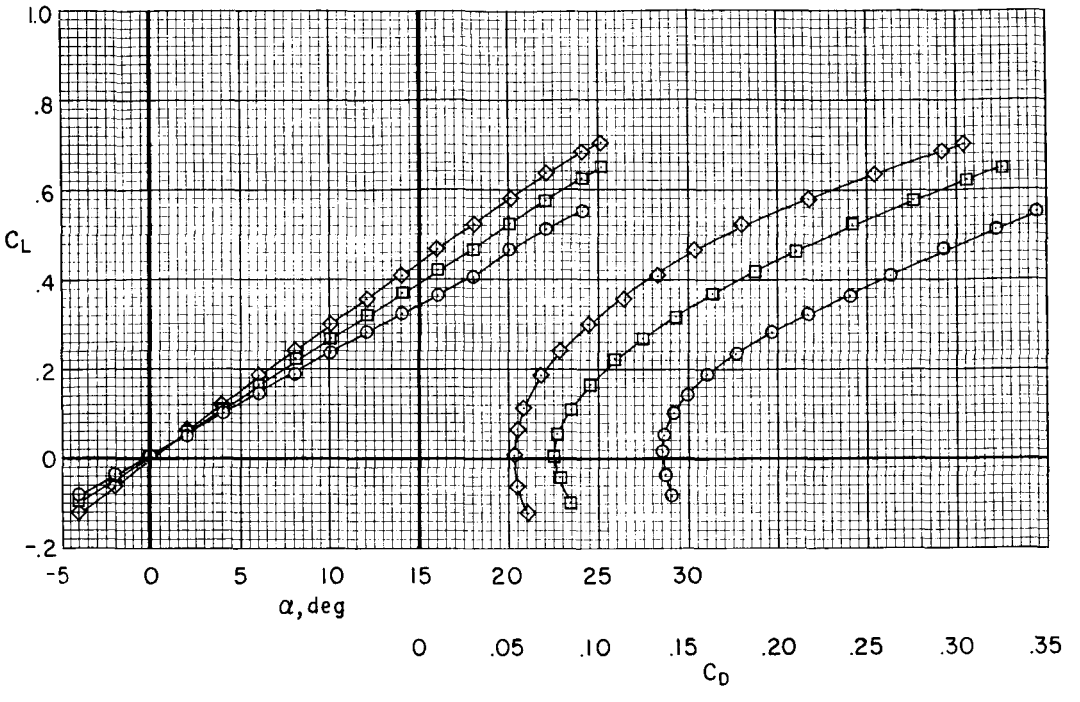

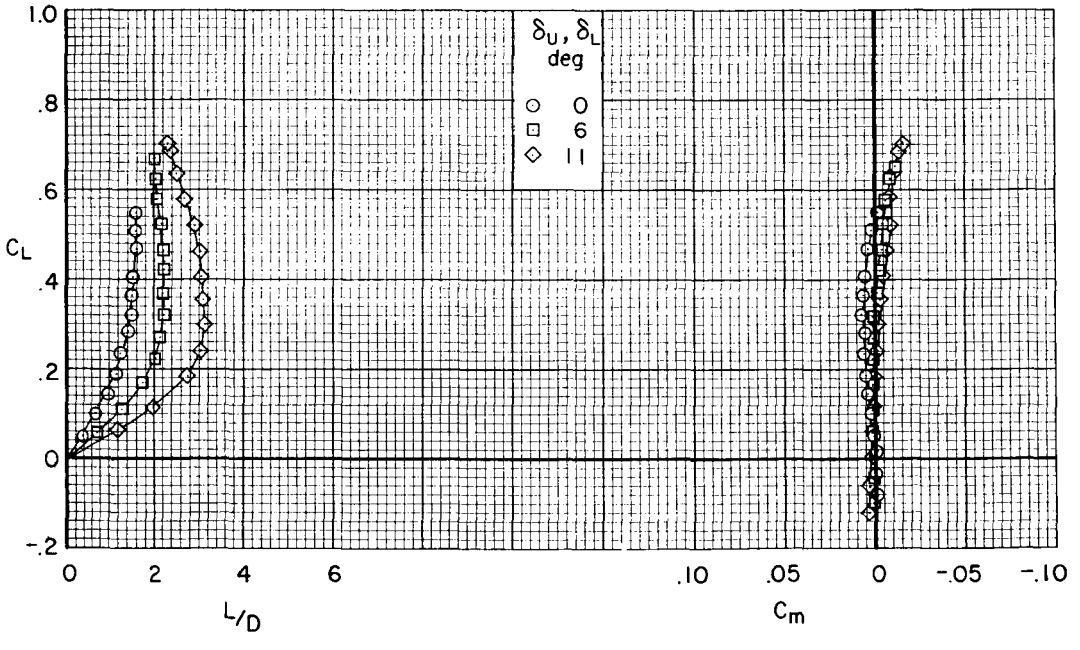

(a) δ_U, δ_L = 0°, 6°, 11°

Figure 7.- The effects of horizontal surface deflection on the low-speed aerodynamic characteristics of the rectangular pyramidal model; M = 0.20; R = 3.3×10^6.

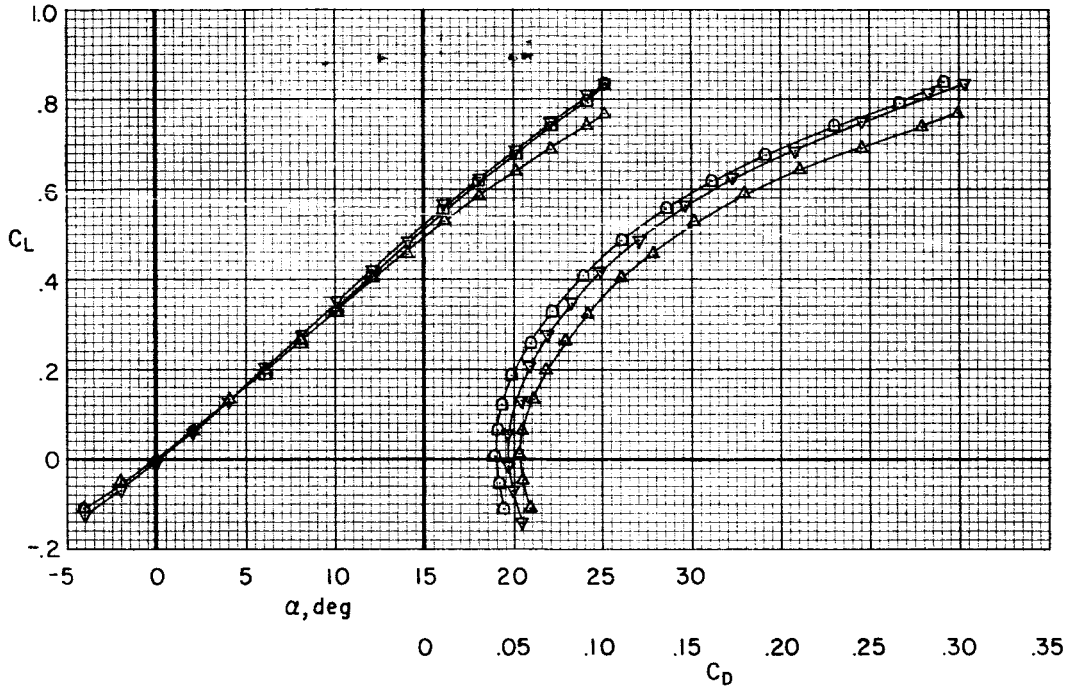

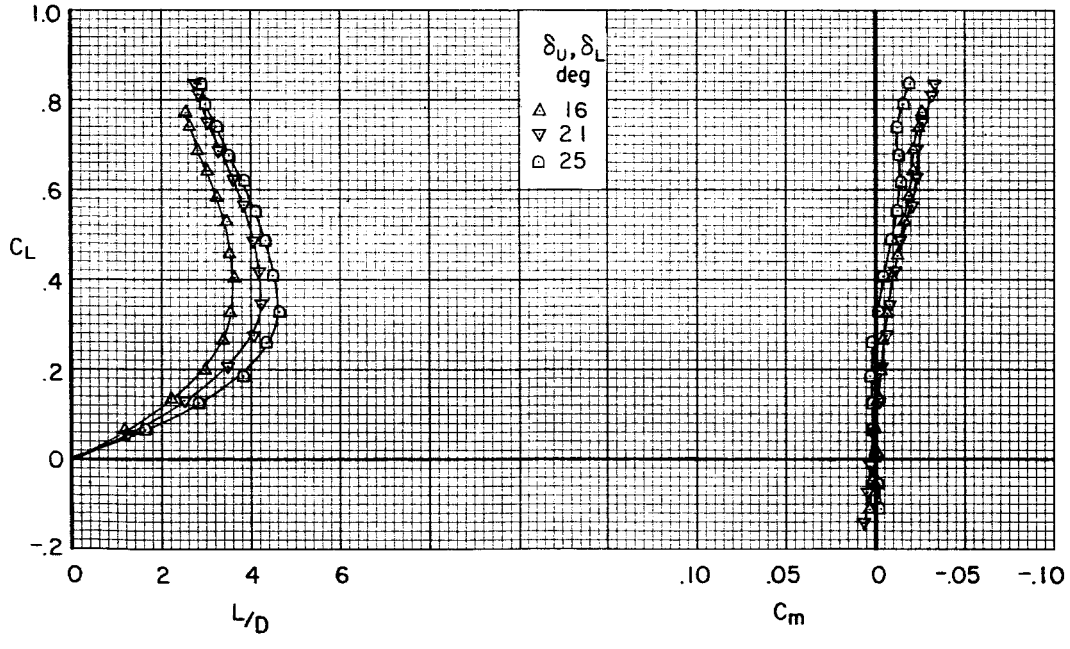

(b) δ_U, δ_L = 16°, 21°, 25°

Figure 7.- Continued.

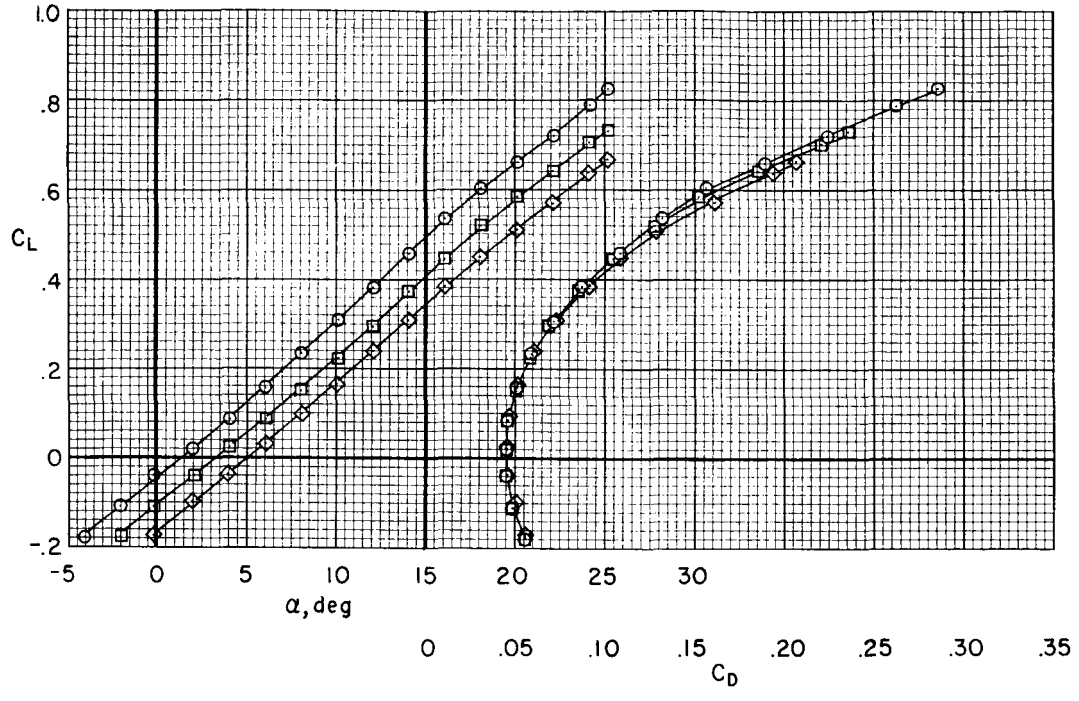

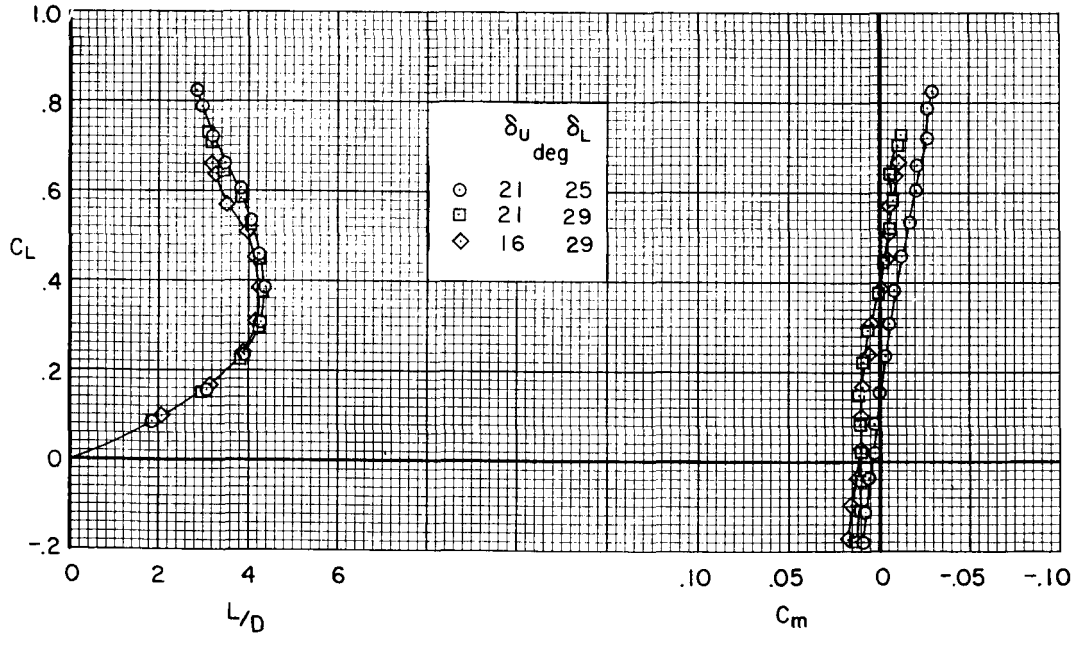

(c) $\delta_U = 21^\circ$, $\delta_L = 25^\circ$; $\delta_U = 21^\circ$, $\delta_L = 29^\circ$; $\delta_U = 16^\circ$, $\delta_L = 29^\circ$; cylindrical sting fairing.

Figure 7.- Concluded.

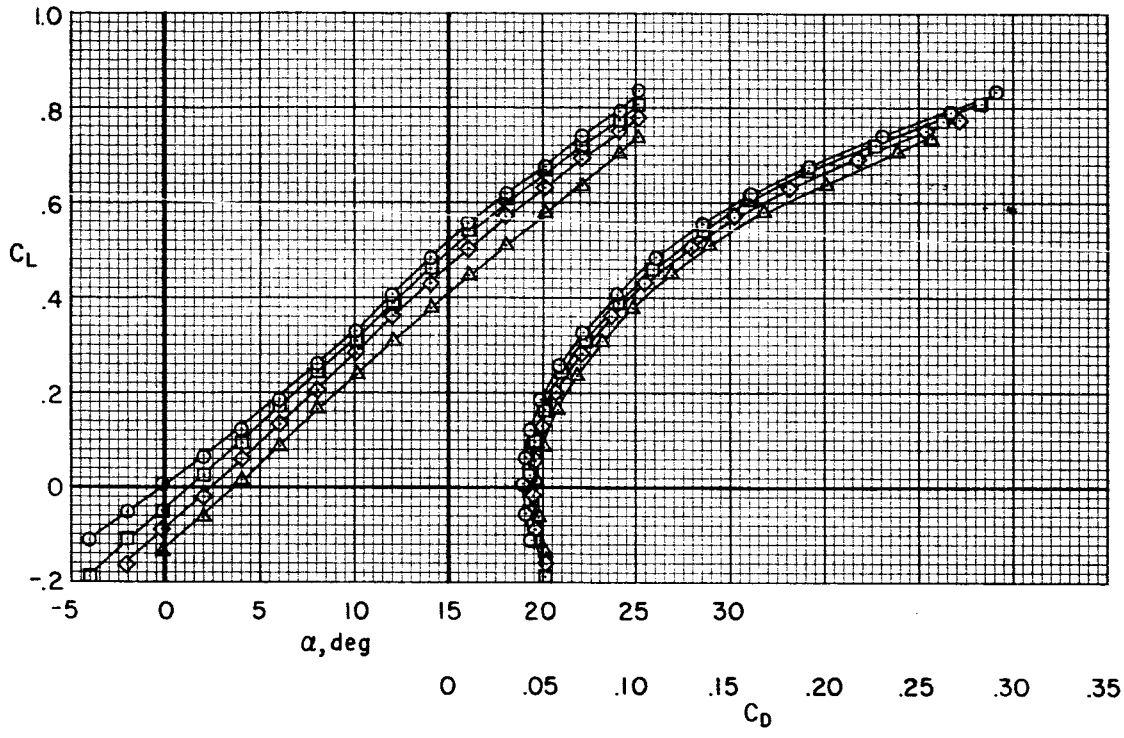

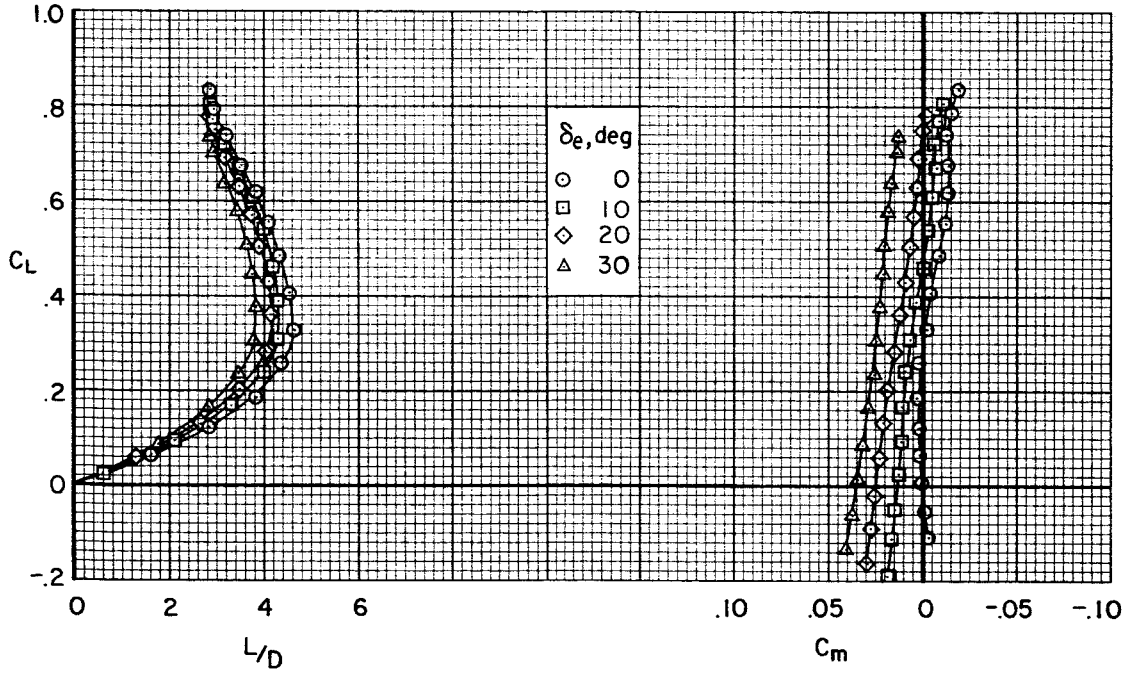

Figure 8.- The effects of elevon deflection on the low-speed aerodynamic characteristics of the rectangular pyramidal model; δ_U, δ_L = 25°; M = 0.20; R = 3.3×10^6.

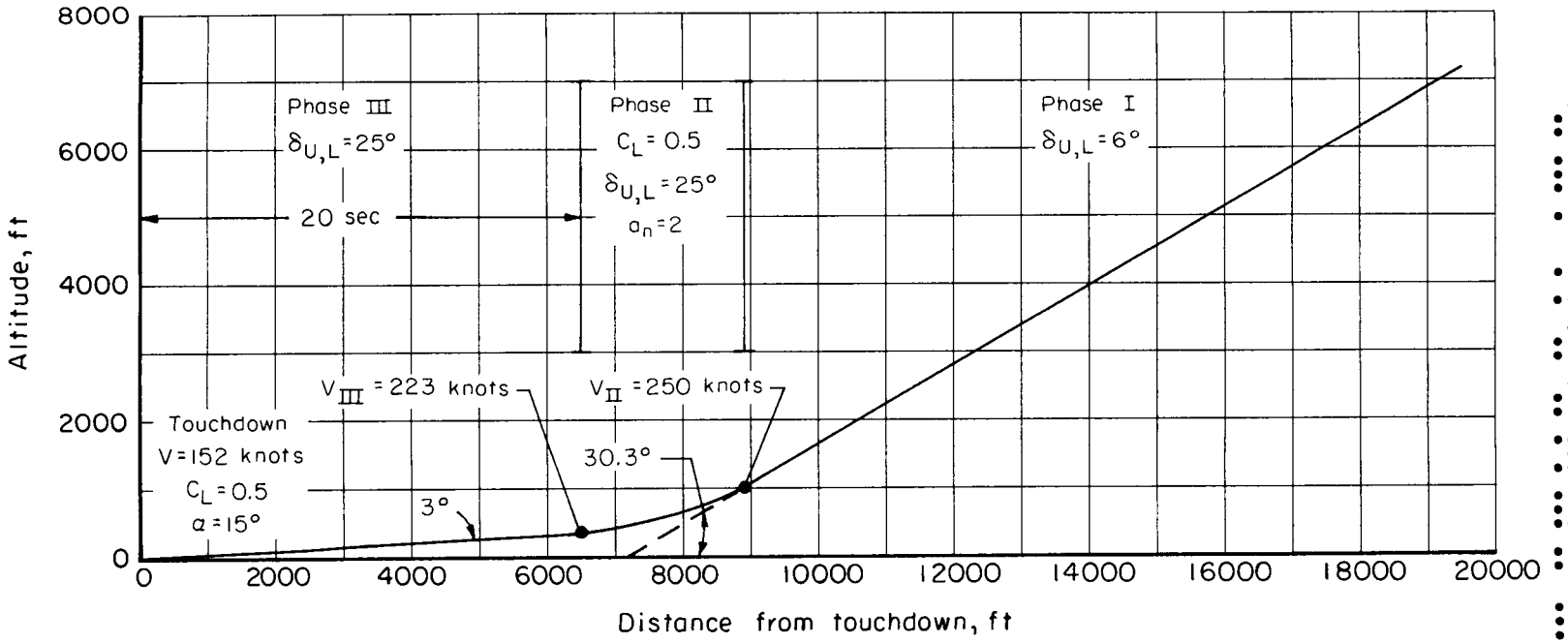

Figure 9.- A landing-approach pattern for a hypothetical re-entry vehicle with wing loading of 40 pounds per square foot.

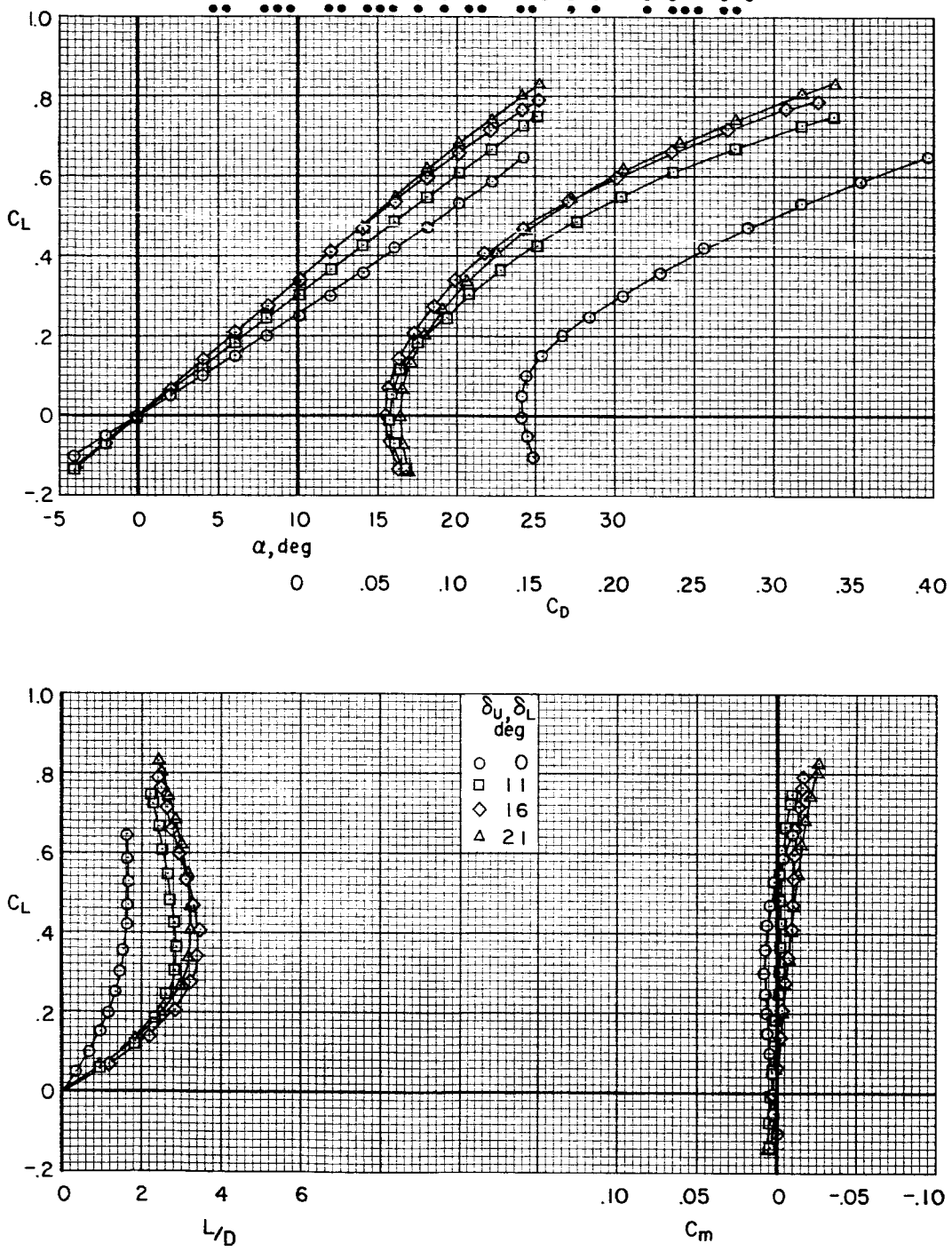

(a) M = 0.60

Figure 10.- The effects of horizontal surface deflection on the high subsonic aerodynamic characteristics of the rectangular pyramidal model; δ_U, δ_L = 0°, 11°, 16°, 21°; R = 3.3×10^6.

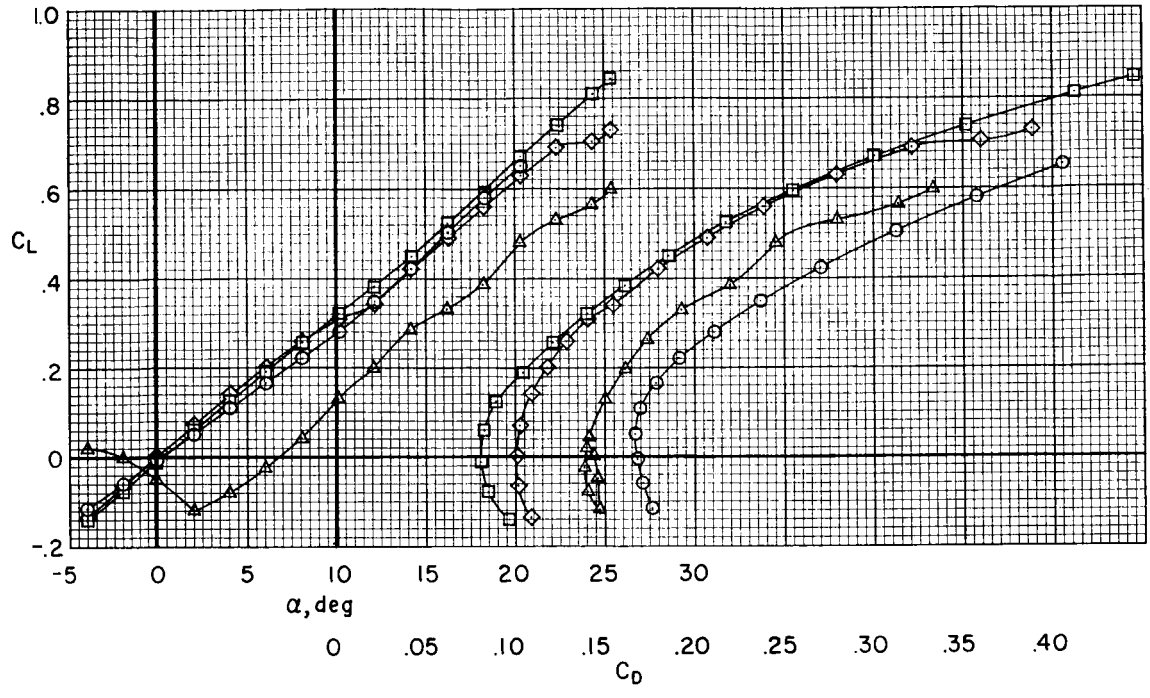

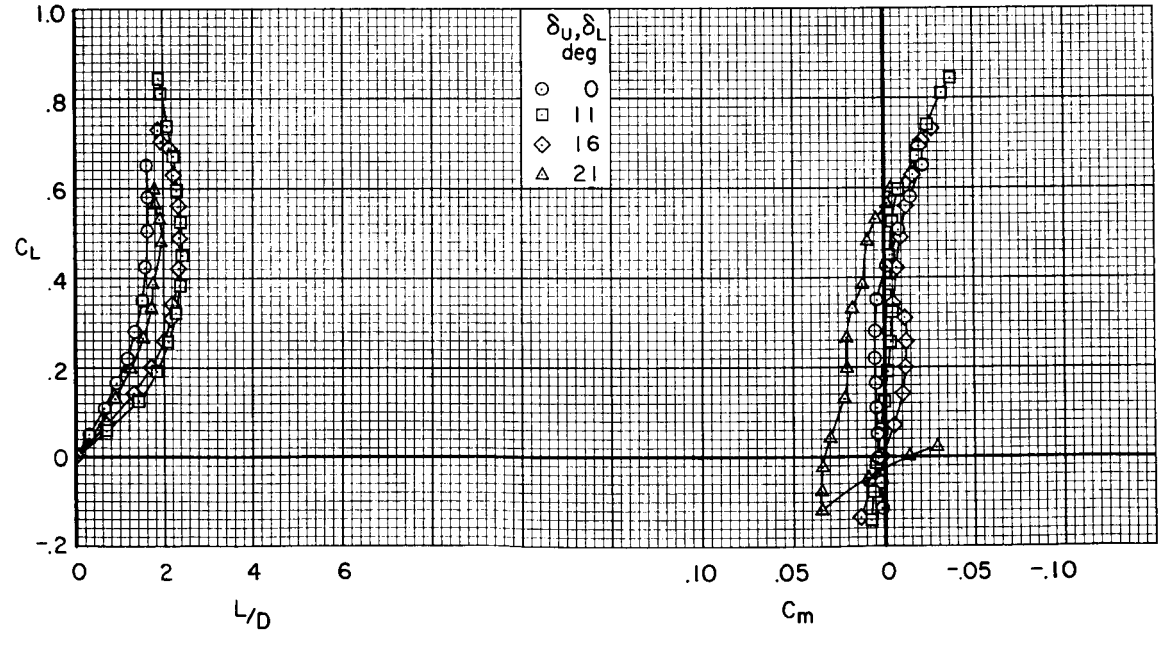

(b) M = 0.80

Figure 10.- Continued.

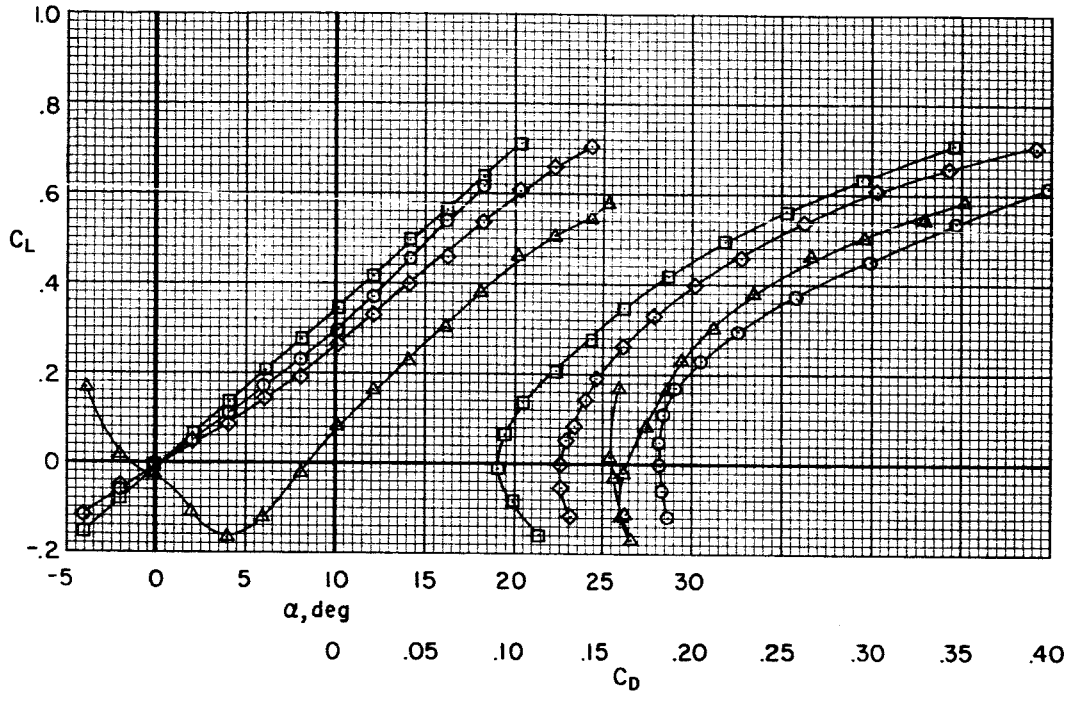

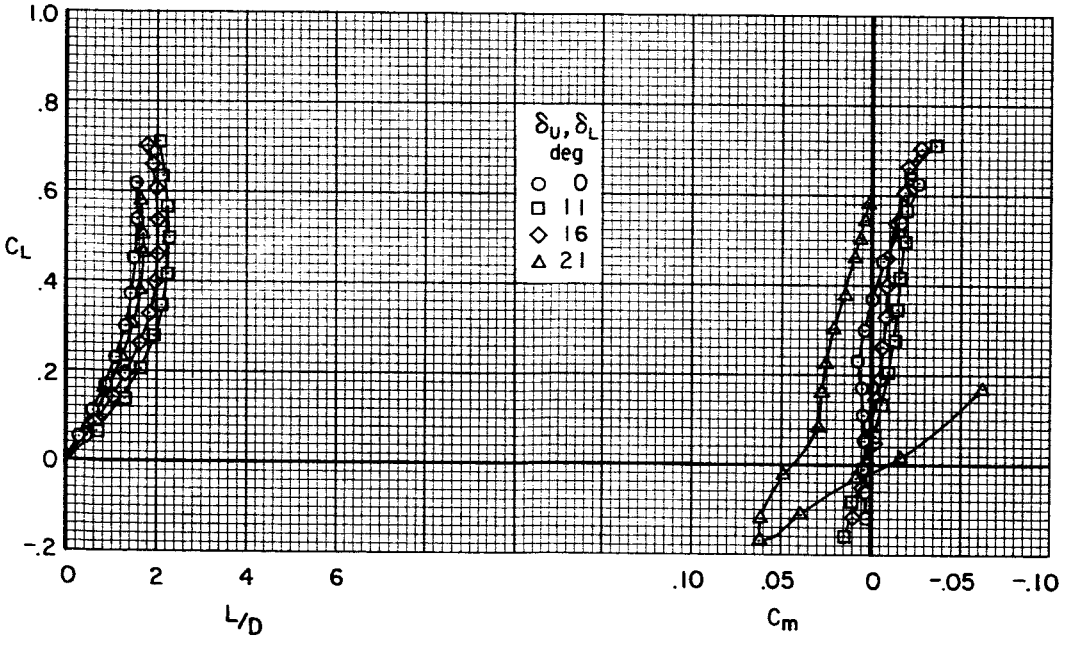

(c) M = 0.85

Figure 10.- Continued.

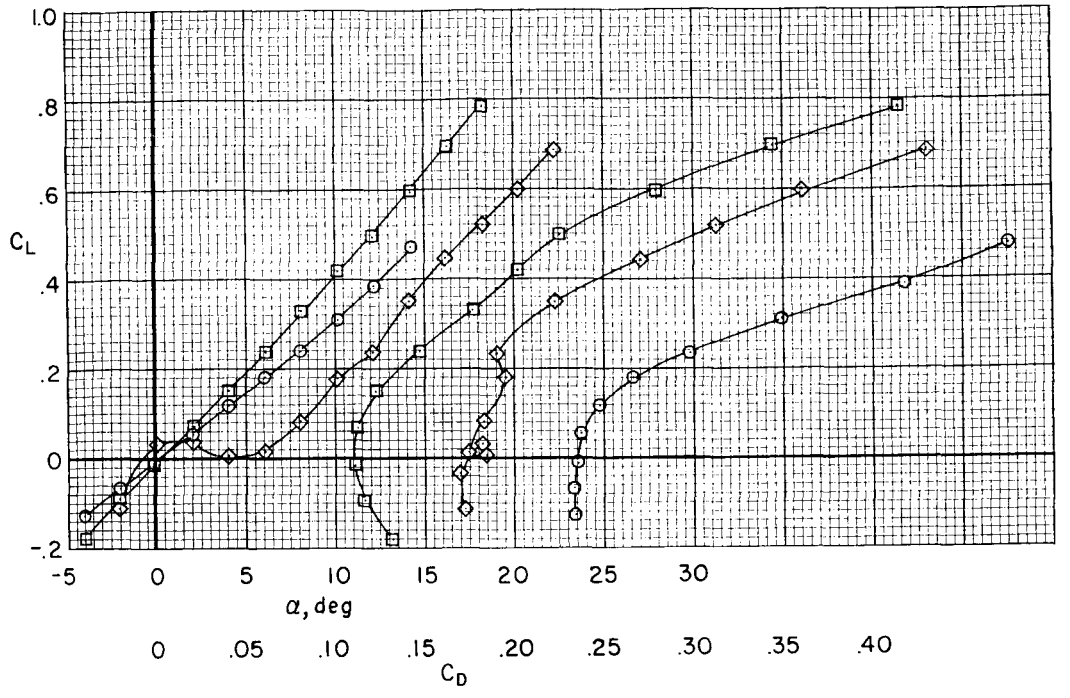

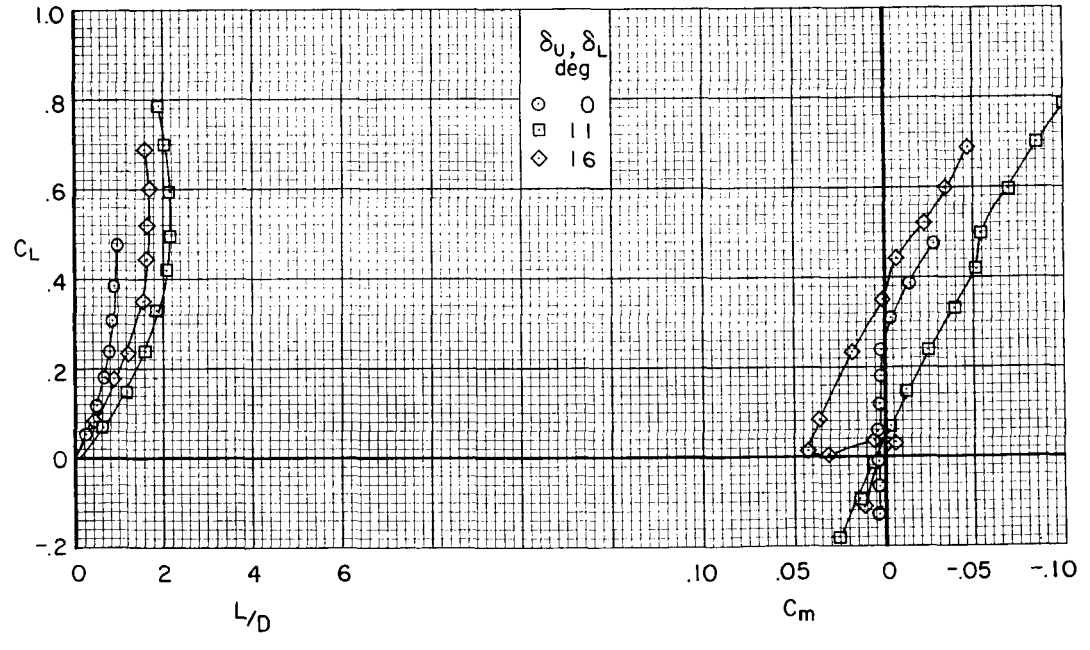

(d) M = 0.90

Figure 10.- Concluded.

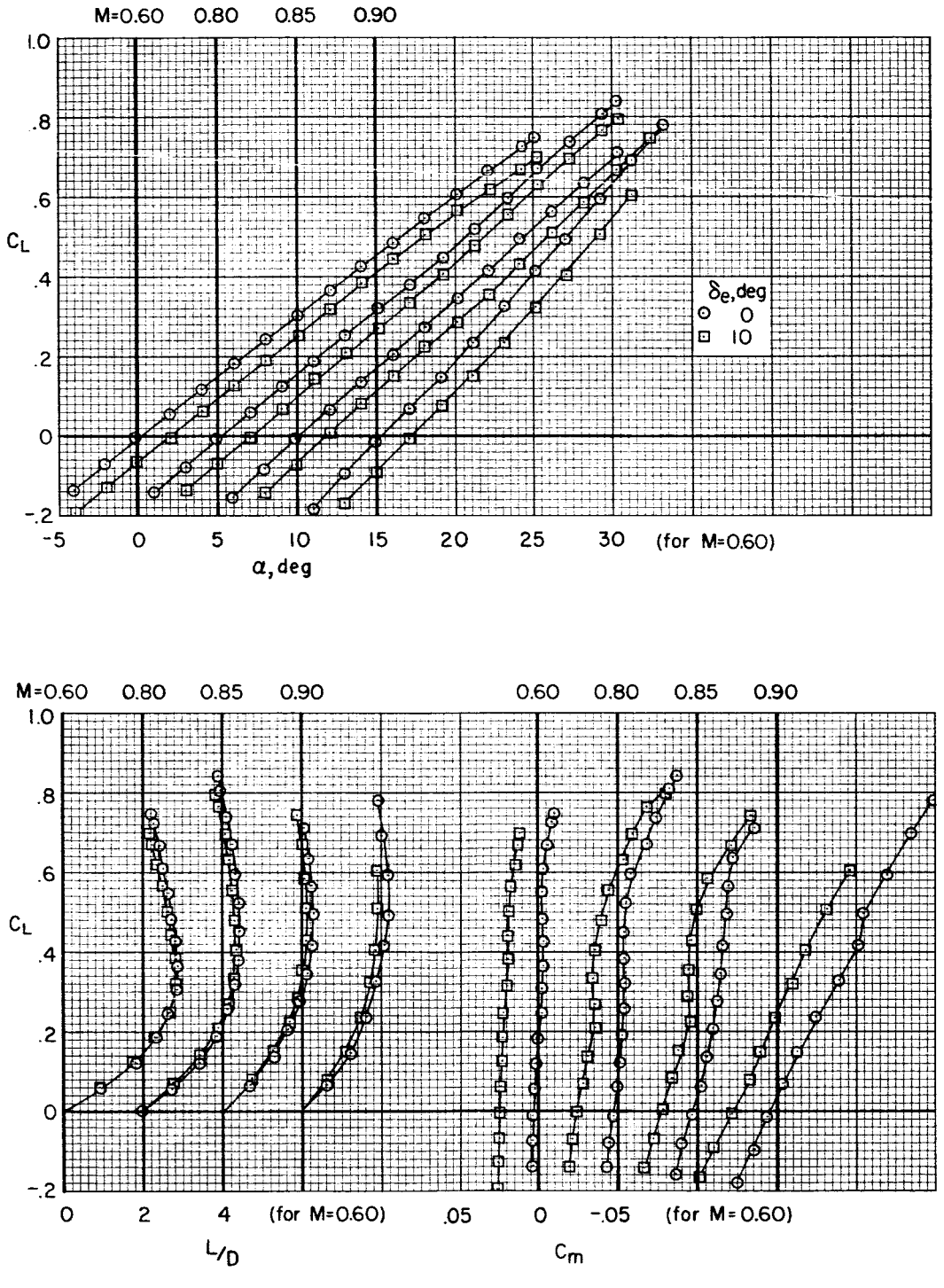

Figure 11.- The effects of elevon deflection on the high subsonic aerodynamic characteristics of the rectangular pyramidal model; δ_U, δ_L = 11°; R = 3.3×10^6.

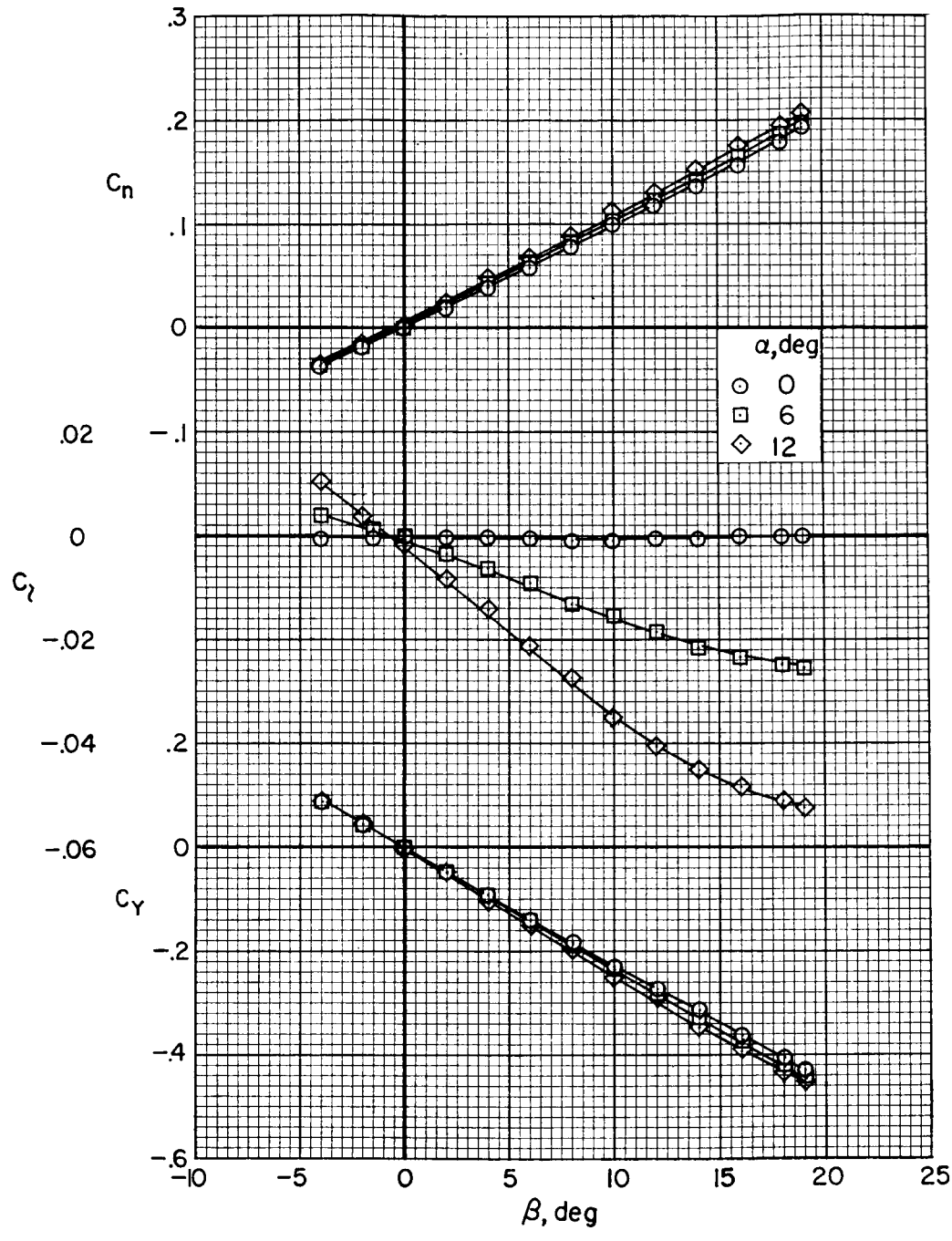

Figure 12.- The low-speed lateral-directional characteristics of the rectangular pyramidal model; δ_U, δ_L = 25°; M = 0.20; R = 3.3×10^6.

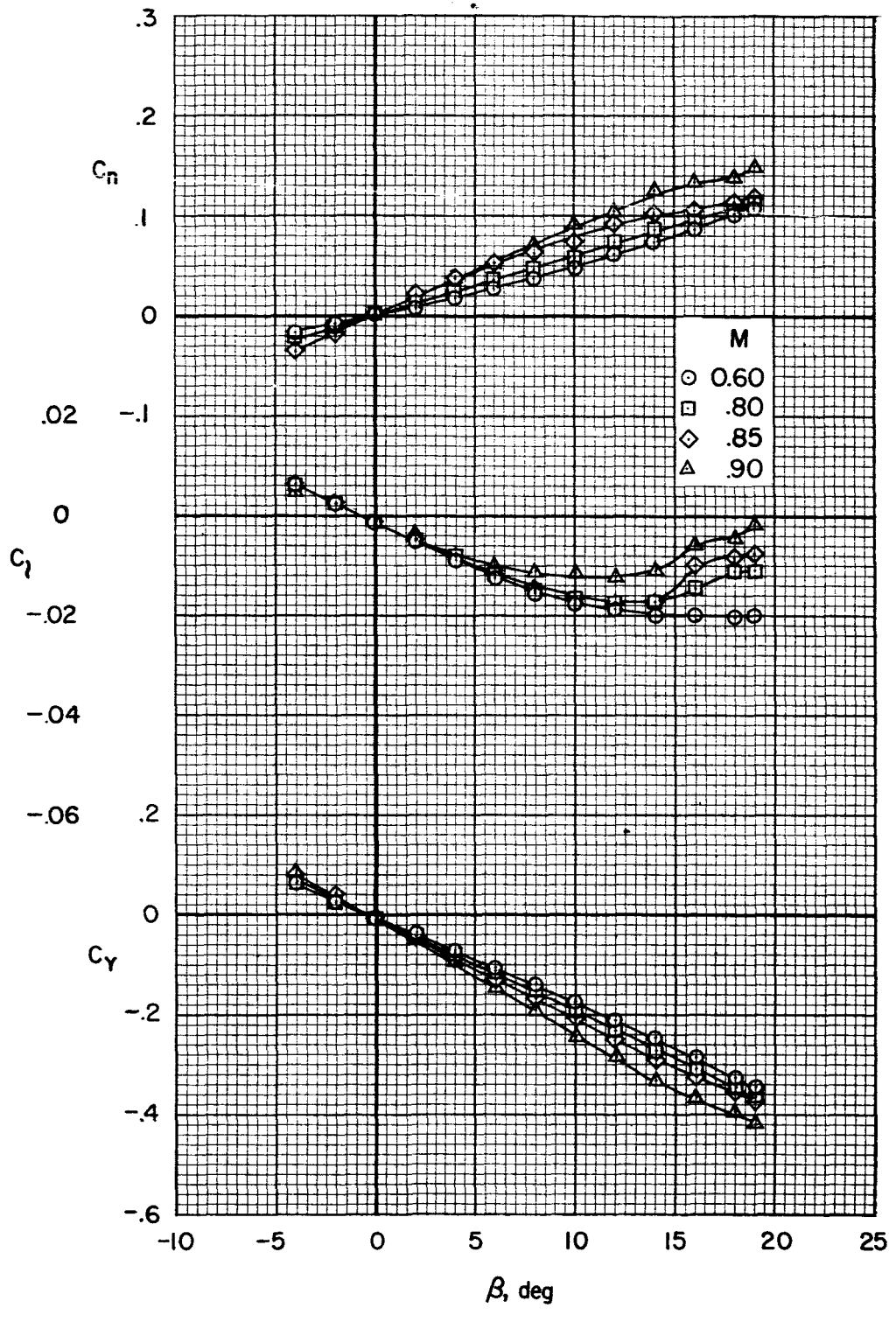

Figure 13.- The high subsonic lateral-directional characteristics of the rectangular pyramidal model; δ_U, δ_L = 11°; α = 6°; R = 3.3X10^6.

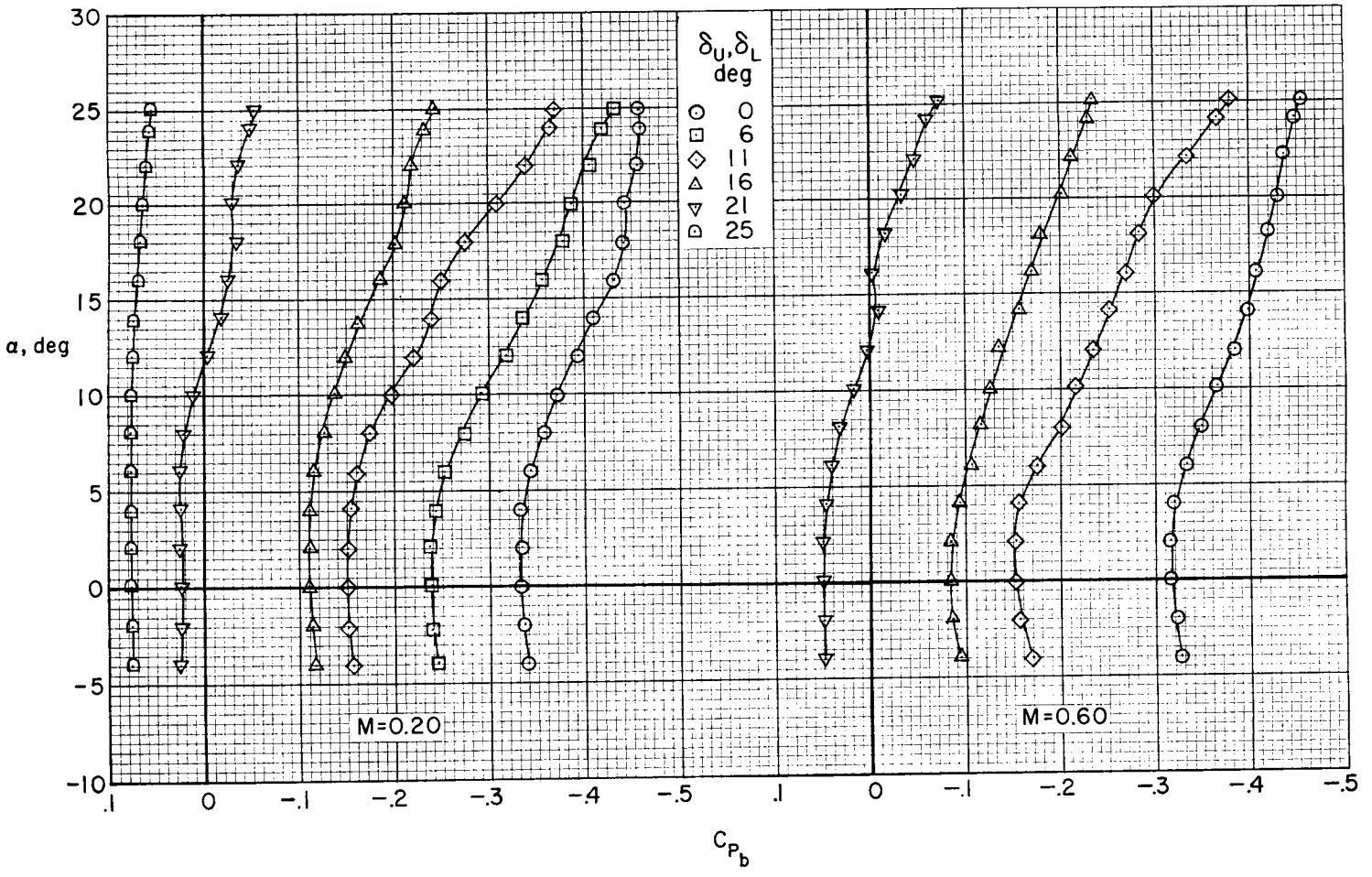

(a) M = 0.20, 0.60

Figure 14.- Base pressures accompanying horizontal surface deflection on the rectangular pyramidal model; R = 3.3×10^6.

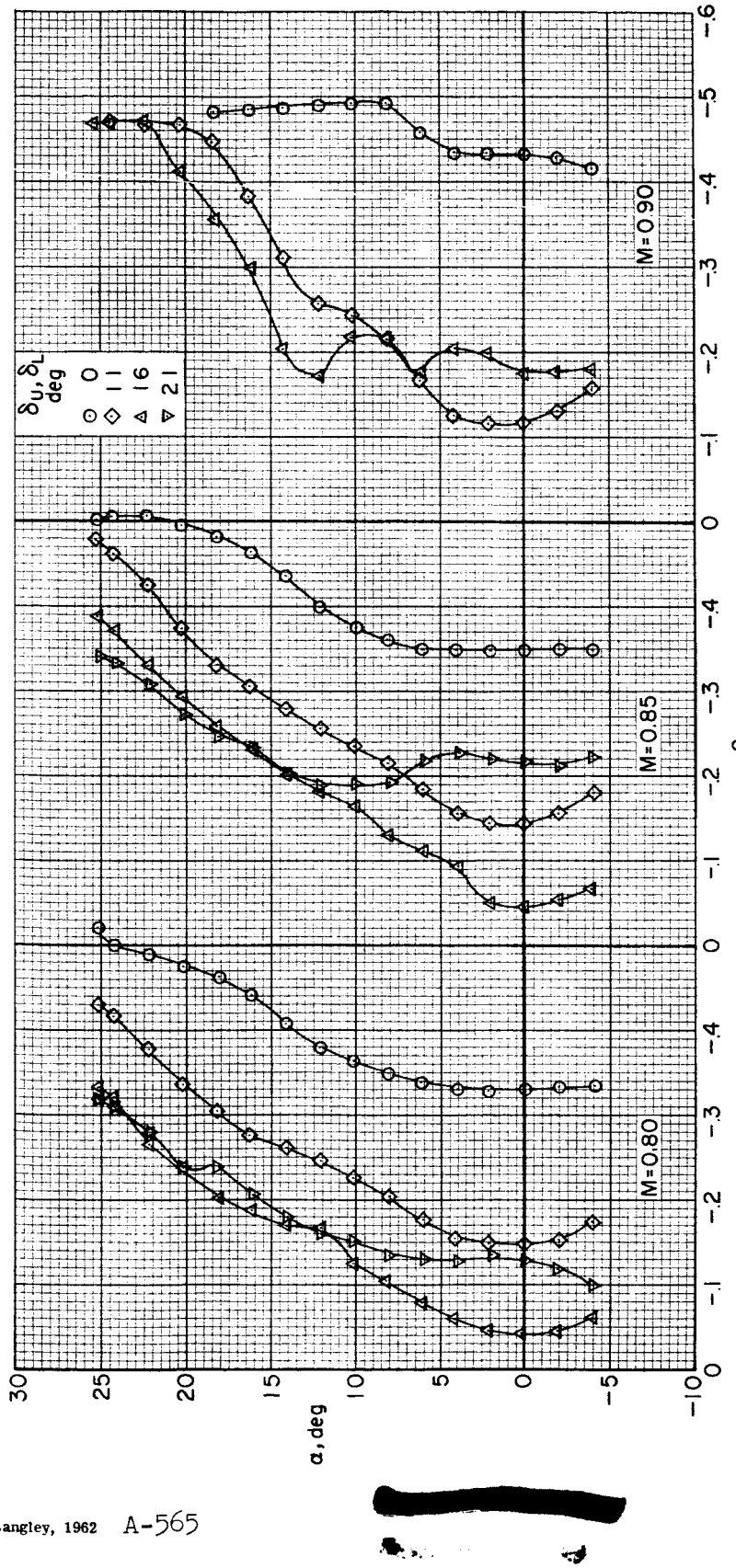

(b) M = 0.80, 0.85, 0.90

Figure 14.- Concluded.